Elucidating a Role for UCP3 in the Control of Mitochondrial Superoxide Flashes

Skye McBride

Supervisor: Dr. Mary-Ellen Harper, Ph.D.

A thesis submitted to the Faculty of Graduate and Postdoctoral Studies in partial fulfillment of the requirements for the degree of Masters of Science in Biochemistry

Faculty of Medicine

Department of Biochemistry, Microbiology and Immunology

University of Ottawa

ABSTRACT:

Mitochondria are a major site of reactive oxygen species (ROS) production in cells. While ROS can cause oxidative damage, they are vital in many signaling processes. Recently, mitochondrial superoxide flashes (mSOF) were defined through sensitive measurements of temporal and spatial differences in superoxide production. mSOF are stochastic events of quantal bursts in superoxide production, which are temporally linked to transient mitochondrial inner membrane depolarizations. The aims of the present study were to characterize a hydrogen peroxide sensitive biosensor to monitor these events and elucidate a role for uncoupling protein 3 (UCP3) and the mechanistic details of mSOF. While pHyPer-dmito was sensitive enough to monitor these dynamic changes its kinetics were insufficient to detect these ~20s long flashes. Additionally, analyses showed a prolonged duration of flashes in the absence of UCP3. Furthermore, we unearthed a novel relationship between flash amplitude and mitochondrial depolarization. Finally, investigations of mSOF in muscles of various fiber type compositions showed no differences, though additional investigations are warranted.

ACKNOWLEDGEMENTS:

First and foremost I would like to thank Dr. Mary-Ellen Harper for her project design and continued support, guidance and encouragement, which created a nurturing environment in which I could further cultivate my abilities as an independent researcher. I am also grateful to Dr. Ryan Mailloux for my initial training and his expertise and input into the design of my project along side Dr. Harper. I would like to thank current and past laboratory members for creating a supporting and fun environment in which I was able to conduct my research.

I would like to thank my Thesis Advisory Committee members. Dr. Steffany Bennett and Dr. Laura Trinkle-Mulcahy, for their input into my project especially in the areas, which at times, were outside of the scope of my knowledge. Some of the analyses would not have been carried out if it were not for their input and continued support.

I would like to show my great appreciation for the training and support I received during my collaboration and time at the University of Rochester in the Dirksen laboratory from Dr. Lan Wei. Without such expertise and hands on training my thesis would not be what it is today. Thank you for putting up with my incessant emails and constant questions.

Additionally, I would like to thank Dr. Lionel Filion and Paul Oleyik for their training and expertise in flow cytometry acquisition, analysis and fluorescence activated cell sorting. Rachel Plewes for her help in organizing and filtering my excel data in R environment and Taran Sachdeva for developing the requisite files for Flash Collector to

operate on Mac OS. A big thanks goes out to Fiona McMurray and Megan MacFarlane for help with conducting final experiments. Finally, I would like to acknowledge the granting agencies for their financial support during my studies.

Current Lab Members
Dr. Mary-Ellen Harper
Dr. Fiona McMurray
Dr. A Brianne Thrush
Brittany Beauchamp
Ghadi Antoun
Georges Kanaan
Jian Xuan
Jessica Quizi
Kijoo Kim
Alyssa Peixoto
Karan Gandhi
Megan MacFarlane

Past Lab Members
Dr. Ryan Mailloux
Dr. Céline Aguer
Cyril Adjeitey
Olivier Charette
Michael Dysart
William Chen
Dhiya Hassan
Linda Jui
Melissa Pasqua

Collaborators and TAC members
Dr. Robert Dirksen
Dr. Lan Wei
Dr. Steffany Bennett
Dr. Laura Trinkle-Mulcahy

Table of Contents

LIST OF ABBREVIATIONS:

A
AA- Antimycotics antibiotics
Ant A- Antimycin A
APS- Ammonium persulfate

B
BCA- Bicinchoninic acid
BMR- Basal metabolic rate
bp- Base pairs
BSA-Bovine serum albumin

C
$CaCl_2$- Calcium chloride
cDNA- Complementary DNA
CHO- Chinese Hamster Ovary cells
CHOEV- Chinese Hamster Ovary cells expressing empty vector
CHOUCP3- Chinese Hamster Ovary cells expressing UCP3
Complex I-NADH:ubiquinone oxidoreductase
Complex II- Succinate Dehydrogenase
Complex III- Coenzyme Q: cytochrome c reductase
Complex IV- Cytochrome C oxidase
Complex V- F_1F_0 ATP synthase
Cyto-Grx1-roGFP2- Cytosol targeted Grx1 conjugated redox sensitive GFP2

D
d- Day(s)
DMEM- Dulbecco's Modified Eagle Medium
DNA- Deoxyribose nucleic acid
DTT- Dithiothreitol

E
ECAR- Extracellular acidification rate
EDTA- Ethylenediaminetetraacetic acid
EGTA- Ethylene glycol tetraacetic acid
EM- Electron microscopy
ETC- Electron transport chain
ETF- Electron transfer flavoprotein
ETF-QO- Electron transfer flavoprotein- ubiquinone oxidoreductase

F
FACS- Fluorescence activated cell sorting
$FAD/FADH_2$- Flavin adenine dinucleotide, oxidized and reduced forms

FBS- Fetal bovine serum
FCCP- Carbonyl cyanide 4-(trifluoromethoxy) phenylhydrazone
FDB- Flexor digitorum brevis
FDHM- Full duration at half maximum
FITC- Fluorescein isothiocyanate
FSC- Forward scatter

G
GFP- Green fluorescent protein
GSH- Reduced glutathione
GSSG- Oxidized glutathione
Grx1- Glutaredoxin 1

H
H^+- Hydrogen ion, proton
H_2O_2- Hydrogen peroxide
HBSS- Hank's balanced salt solution
HCl- Hydrochloric acid
HEPES- 2-[4-(2-hydroxyethyl)piperazin-1-yl]ethanesulfonic acid
HEK293- Human embryonic kidney cells
h- Hour(s)
HRP- Horseradish peroxidase
Hz- Hertz

I
IR- Insulin Resistance

K
kb- Kilobase
KCl- Potassium chloride
kDa- Kilo Dalton
KH_2PO_4- Potassium phosphate

L
L- Liter
LB- Lysogeny broth

M
µM- Micromolar
M- Molar
mg- Milligram
$MgCl_2$- Magnesium chloride
$MgSO_4$- Magnesium sulfate
MHC- Myosin heavy chain
MIM- Mitochondrial inner membrane
min- Minute(s)
mito-Grx1-roGFP2- Mitochondrial targeted Grx1-roGFP2

mL- Milliliter
mM- Millimolar
MOM- Mitochondrial outer membrane
mSOF- Mitochondrial Superoxide Flash
mt-cpYFP- Mitochondrial targeted circularly permuted YFP
MTT- 3-(4,5-dimethylthiazol-2-yl)-2,5-diphenyltetrazolium bromide

N
NaCl- Sodium chloride
NAD^+/NADH- Nicotinamide adenine nucleotide, oxidized and reduced forms
$NaHCO_3$- Sodium bicarbonate
Nm- Nanometer
NP-40- Tergitol-type nonyl phenoxypolyethoxyethanol

O
O_2- Molecular oxygen
$O_2^{\cdot-}$- Superoxide
OCR- Oxygen consumption rate
OXPHOS- Oxidative phosphorylation

P
PAGE- Polyacrylamide gel electrophoresis
PFA- Paraformaldehyde
pH- Power of hydrogen
pHyPer-dmito- Mitochondria targeted hydrogen peroxide circularly permuted YFP
P_i- Inorganic phosphate
PMF- Protonmotive force

R
RNS- Reactive nitrogen species
ROS- Reactive oxygen species
RIPA-Radio-Immunoprecipitation Assay
roGFP2- Redox sensitive GFP
ROI- Region of interest
RRR- Regular rodent ringer

S
s- Second(s)
SD- Standard Deviation
SDS-Sodium dodecyl sulfate
SEM- Standard error of the mean
SSC- Side scatter
State 3- ADP stimulated respiration
State 4- Leak dependent respiration
State 4_o- Oligomycin induced respiration due to leak

T
TBS- Tris buffered saline solution
TBS-T- Tris-buffered saline containing 1% (v/v) Tween-20
TCA- Tricarboxylic acid
TEMED- N,N,N',N'-tetreamethyleethane-1,2-diamine
TMRE- Tetramthylrhodamine, Ethyl Ester Perchlorate
Tris- Trisaminomethane

U
UCP- Uncoupling protein
UCP3KO- Uncoupling protein 3 knockout

V
v/v- Volume per volume
V- Volts

W
WT- Wildtype
w/v- Weight per volume

X
xg- Centrifugal force

Y
YFP- Yellow fluorescent protein

Symbols
~ - Approximately
ΔG - Gibbs free energy

LIST OF FIGURES:

1.0 GENERAL INTRODUCTION:

1.1 Context

This thesis focuses on stochastic bursts in mitochondrial reactive oxygen species (ROS) emission and the characterization of regulatory mechanisms. The latter phenomenon is referred to as mitochondrial superoxide flashes (mSOF). Cellular ROS levels exist as a balance between ROS production and detoxification. Originally, ROS were considered to be solely toxic due to their reactive nature with DNA, lipids, proteins and other biomolecules causing oxidative damage (Murphy, 2009). More recently the identification of ROS as signaling molecules has opened new doors in ROS and mitochondrial research. Specifically, impaired ROS handling has been associated with disease states including obesity and diabetes and thus an improved understanding of ROS is relevant to potential preventative and therapeutic aspects for diseases that are currently of great concern internationally.

1.2 Aerobic respiration and oxidative phosphorylation (OXPHOS)

While mitochondria partake in a variety of processes including maintenance of calcium homeostasis, apoptotic signaling and concerted mechanisms regulating nuclear gene transcription, their main role is cellular energy transduction (Chang et al., 2013; Chen et al., 2012; Gellerich et al., 2013). Cellular ATP production is driven by fuel oxidation resulting in the conversion of the Gibbs free energy (ΔG) stored in the bonds of these fuels to the cellular energy currency ATP. Carbohydrates, lipids and proteins are oxidized through glycolysis, β-oxidation and amino acid metabolism, respectively, ultimately resulting in the generation of key metabolic intermediates, which drive the tricarboxylic acid (TCA) cycle. It is the TCA cycle, which is responsible for the generation of the majority of the reduced coenzymes,

NADH+, H^+ and $FADH_2$, ultimately driving ATP production via electron donation to the electron transport chain (ETC) (Bayir and Kagan, 2008; Scialo et al., 2013). Alternative pathways for electron donation exist, including electron transfer from fatty acid metabolism to electron transfer flavoprotein (ETF) and subsequently through ETF oxidoreductase (ETF:QO) to the electron transport chain (Rinaldo et al., 2002).

Energy transduction by the oxidative phosphorylation (OXPHOS) system was first explained by Peter Mitchell's chemiosmotic theory. This theory is based on the described coupling of electron transfer producing an electrical gradient and a chemical gradient from which energy is harnessed in the form of ATP (Mitchell, 1966; Mitchell, 1972; Sluse, 2012; Mitchell, 1961). Energy transduction by OXPHOS, located in the mitochondrial inner membrane (MIM), is driven by the difference in redox potential across the electron transport chain, spanning 1.14V, which drives the stepwise transfer of electrons (also referred to as reducing equivalents) through the respiratory complexes (I-IV) to the final electron accepter, molecular oxygen (O_2) (Schagger et al., 2004; Madeira, 2012; Brand and Nicholls, 2011). It is this redox gradient, which involves the complementary process by which concomitant reduction and oxidation reactions take place, that allows the transfer of electrons within complexes through flavin (CI) and prosthetic groups (CI, II, III) as well as iron-sulfur clusters (CI, II, III) and copper-sulfur clusters (CIV) found within the respiratory complexes (Jastroch et al., 2010; Brand et al., 2005).

Briefly, reducing equivalents enter the ETC from the oxidation of substrates to reduce NADH-coenzyme Q reductase (Complex I) and succinate dehydrogenase (Complex II). These two complexes then reduce ubiquinone, a lipophilic electron carrier, to ubiquinol

(Schagger et al., 2004). These reducing equivalents then transfer electrons to cytochrome c oxidoreductase (Complex III) and subsequently reduce cytochrome c located on the cytoplasmic side of the MIM. Cytochrome c shuttles the electrons to cytochrome c oxidase (Complex IV) and finally electrons are donated to O_2 reducing it to water (Mailloux and Harper, 2011; Gunner et al., 2008).

This shuttling of electrons drives the simultaneous transport of H^+ ions out of the mitochondrial matrix into the intermembrane space. Such transport results in the creation of an electrochemical gradient across the MIM, which is of central importance in the chemiosmotic theory (Mitchell, 1961; Mitchell, 1966; Mitchell, 1972; Mitchell, 2011). This electrochemical gradient is more commonly referred to as the protonmotive force (PMF). PMF is the driving force behind ATP production by F_0F_1 ATP synthase. ATP synthesis occurs as protons reenter the mitochondrial matrix by traveling down their concentration gradient through the F_0 subunit of ATP synthase to the matrix (Mitchell, 1972; Mitchell, 2011) (Figure 1).

1.3 Uncoupled respiration

While the generation of stored energy in the form of a PMF across the MIM is essential for the production of ATP via F_0F_1 ATP synthase, the supply and demand of these two processes is not always equal. Because of this an apparently adaptive mechanism by which protons passively reenter the mitochondrial matrix independent of ATP synthesis is present. This process is referred to as uncoupled oxidative phosphorylation since oxidation of fuels and the generation of PMF does not translate to ATP synthesis (Figure 1). This process

Figure 1

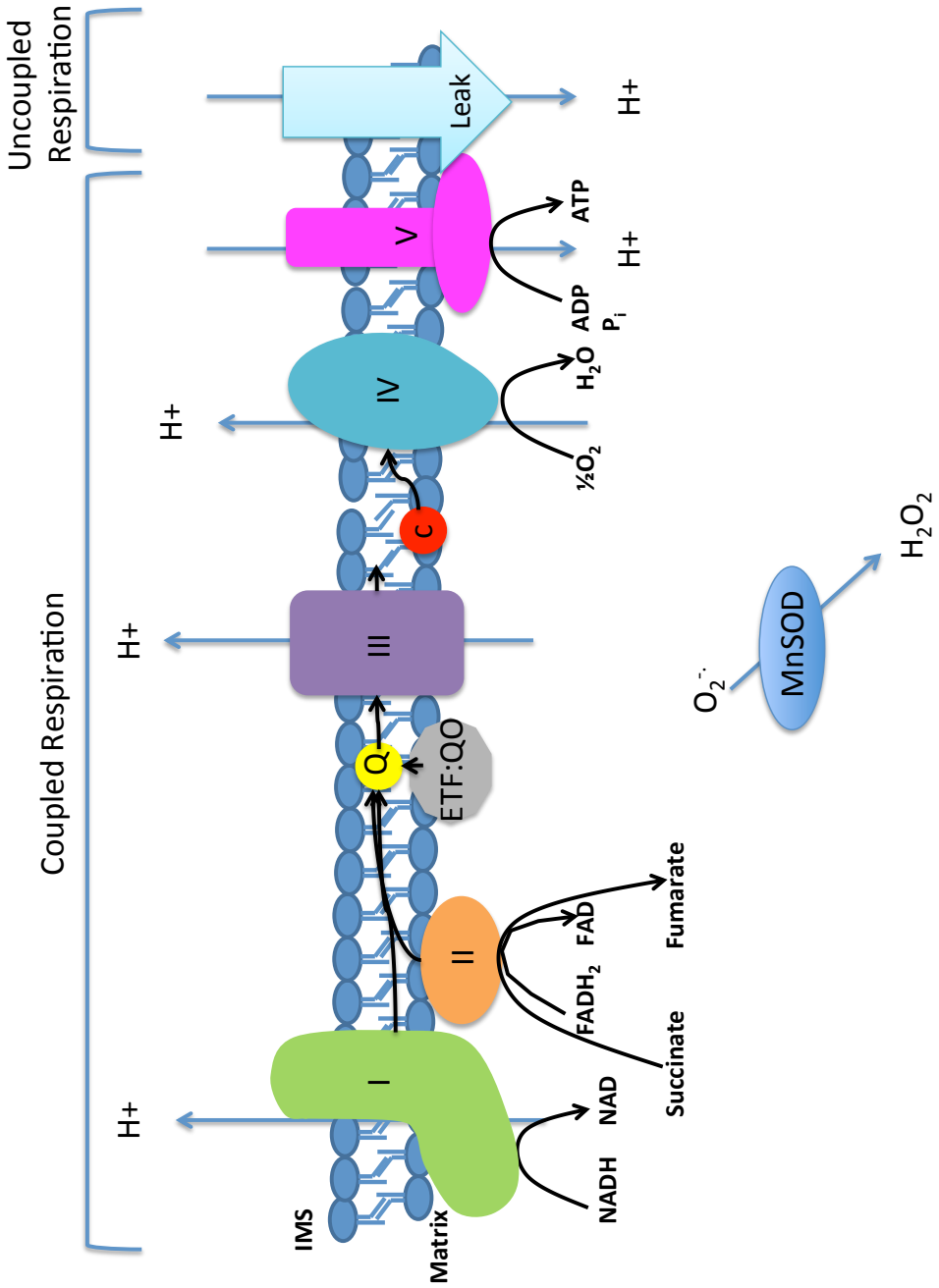
Uncoupled Respiration
Coupled Respiration
Leak
H+
V
ATP
ADP
P_i
H+
IV
H_2O
$½O_2$
H+
c
III
H+
Q
ETF:QO
II
FAD
$FADH_2$
Fumarate
Succinate
I
NAD
NADH
IMS
Matrix
$O_2^{\cdot-}$
MnSOD
H_2O_2

Figure 1- Oxidative Phosphorylation under "coupled" and "uncoupled" states. Coupled oxidative phosphorylation occurs when respiration is coupled to the synthesis of ATP synthesis. The transfer of reducing equivalents through complexes (I-IV) of the electron transport chain drives the pumping of hydrogen ions (H^+) from the matrix to the intermembrane space producing a proton gradient. This gradient is used to drive ATP production by the F_oF1 ATP synthase. During uncoupled respiration, protons leak back (down their concentration gradient) through leak mechanisms, i.e., via uncoupling protein-3 (UCP3), adenine nucleotide translocator (ANT) or phosphate carrier into the mitochondrial matrix. Leaks through UCP3 are a ROS detoxification mechanism. This mechanism is initiated by the production of superoxide ($O_2^{\cdot-}$) a by-product of coupled respiration. Superoxide is produced by electron slippage and is dismutated into hydrogen peroxide (H_2O_2) by the matrix enzyme manganese superoxide dismutase (MnSOD).

is also referred to as mitochondrial proton leak. This proton leak is thought to occur in one of two general ways (basal or inducible).

Basal uncoupling is not regulated, is thought to occur in all tissue types and is associated with the basal metabolic rate (BMR) of the organism. For example, in skeletal muscle up to 50% of the measured basal oxygen consumption rate can be attributed to proton leak mechanisms (Rolfe and Brand, 1996a; Rolfe et al., 1999). On a whole body scale, leak respiration can account for nearly 25% of BMR (Rolfe and Brand, 1996b; Rolfe et al., 1999; Brand et al., 1999). Proton leak respiration is highest within the mitochondria when substrate is available (high PMF) but ATP demand is low. A high proportion of this basal leak can be attributed to the adenine nucleotide translocator (ANT) (Rolfe and Brand, 1996b; Brand et al., 2005b).

Furthermore proton leak mediated respiration may be induced through activation of ANT or uncoupling proteins (UCPs) directly by fatty acids, reactive alkenes or ROS (Echtay et al., 2002; Echtay et al., 2003). In addition, natural inhibitors of these transmembrane proteins exist such as purine nucleotides, including ADP and GDP, carboxyatractyloside and bongkrekic acid (Garcia et al., 2000; Ricquier et al., 1982). However, the usefulness of these inhibitors is limited due to the non-specific nature of their effects (*e.g.*, GDP inhibits UCPs and ANT) (Brand et al., 2005b).

1.4 Uncoupling protein 3 (UCP3)

Uncoupling proteins (UCPs) 1-5 belong to the anion carrier protein superfamily (Affourtit et al., 2007). These proteins, while similar in sequence, structure, location in the

MIM and ability to cause leak, their expression patterns and physiological functions within the cell vary. UCP1 is expressed solely in brown adipose tissue and its activation and proton leak functions play a role in adaptive thermogenesis for the physiological function of thermoregulation (Himms-Hagen, 1990; Himms-Hagen, 1989; Matthias et al., 1999). The amino acid sequence homology between UCP1 and the so-called novel UCPs, UCP2 and UCP3 is approximately 59% (Ricquier and Bouillaud, 2000). UCP2 and 3 however, share approximately 73% sequence homology to each other and their function is required for modulating the PMF of the MIM in order to mitigate ROS production (Bray and Ryan, 2012; Boss et al., 1997; Fleury et al., 1997; Ricquier and Bouillaud, 2000b; Vidal-Puig et al., 1997). While UCP2 is expressed in the spleen, thymus, pancreas and certain neuronal cells, UCP3 expression is restricted to skeletal muscle, brown adipose tissue and heart (Costford et al., 2006; Ricquier and Bouillaud, 2000b; Estey et al., 2012). UCPs 4 and 5 have been identified at the transcript level in brain and to a lesser extent in heart, lung, skeletal muscle, kidney and liver; however, detection at the protein level has not been possible and information about their functions has not been extensively studied (Mao et al., 1999; Lengacher et al., 2004; Yu et al., 2000; Sanchis et al., 1998). Hereafter the focus will be on UCP3 since it is the only UCP expressed at the protein level in skeletal muscle, the tissue studied in this thesis.

UCP3 was first identified using a homology-based screening method comparing its sequence to that of UCP1 and UCP2 (Boss et al., 1997). The UCP3 gene, located on chromosome 7 in mice and chromosome 11q13 in humans, encodes both a short and long isoform encoding the same first 275 amino acids. While the there is exists no evidence that the short isoform is translated into protein the full length protein containing 312 amino acids

and weighing ~34kDa protein (Boss et al., 1997). UCP3 spans the mitochondrial inner membrane forming a pore allowing for H^+ ions (and perhaps other ions) to selectively pass through. Based on its homology to UCP2, its pore is formed from six predicted alpha-helical transmembrane domains (Berardi et al., 2011) . Like other UCPs, it is thought to function in the form of a dimer.

While the requisite binding domains for UCP activation by fatty acids and inhibition by purine nucleotide are poorly understood, mechanisms for UCP3 activity regulation have, to some extent, been elucidated. It was Echtay et al. that provided evidence for the first mechanism for self-regulating UCP activation by superoxide in the control of mitochondrial ROS production (Echtay et al., 2003; Echtay et al., 2002). More recently, our laboratory has shown that UCP3 can be turned on and off in response to changes in ROS levels through a mechanism that involves reversible glutathionylation reactions with two key cysteine residues, Cys25 and Cys259 (Mailloux et al., 2011). Specifically it has been shown that under conditions of increased ROS production UCP3 is deglutationylated resulting in its activation. Deglutathionylated, or activated, UCP3 is then able to decrease the PMF through proton reentry to the mitochondrial matrix. A reduction in PMF decreases ROS emissions promoting UCP3 deactivation via protein (Mailloux and Harper, 2011; Mailloux et al., 2011). This process involves glutaredoxin-2, a mitochondrial targeted glutathione transferase enzyme.

As mentioned, the main physiological function of UCP3 is thought to lie in its ability to mitigate ROS production and control energy expenditure through leak mechanisms (Affourtit et al., 2007; Harper et al., 2008). As a result of its restricted expression,

specifically in skeletal muscle, UCP3 has the ability to affect whole body energy expenditure given the high metabolic activity of this tissue. Increases in UCP3 expression have been linked to enhanced FA uptake, transport and metabolism (Hoeks et al., 2003; Bezaire et al., 2005). Chronic exposure to FA as a result of these associations has been shown to regulate UCP3 at both the transcript and protein level in rodents and humans (Hoeks et al., 2003). In support of these findings UCP3 expression has been shown to decrease the respiratory exchange ratio a marker for FAO (Bezaire et al., 2005). Similarly, mutations in UCP3 protein have been implicated in impaired FAO with reductions of up to 50% on a whole body level as well as observed elevations in the measured non-protein respiratory quotient compared to individuals expressing the non-mutant protein (Argyropoulos et al., 1998; Argyropoulos and Harper, 2002).

The role for UCP3 in uncoupling has been supported by associations with obesity, weight loss and insulin sensitivity in a variety of studies. In a cohort of obese women undergoing a diet induced weight loss program analyses showed that a greater rate of weight loss correlated with increased levels of UCP3 transcripts in the rectus femoris muscle and 50% greater proton leak respiration in mitochondria that were isolated from this quadriceps muscle (Harper et al., 2002). Similarly, overexpression of UCP3 in muscle of mice has been associated with protection from weight gain, increased insulin sensitivity as well as general improvements in an assortment of metabolic parameters (Affourtit et al., 2007; Bezaire et al., 2005; Harper et al., 2001). The opposite trend has been observed in UCP3KO models where its absence has shown increased tendency towards diet induced obesity and decreased insulin secretion with implications of T2DM on a whole body level with T2DM patients showing decreased mRNA and protein levels (Costford et al., 2008; Mailloux et al., 2010; Mailloux et

al., 2012a; Song et al., 2012; Chan and Harper, 2006; Krook et al., 1998; Schrauwen et al., 2001; Schrauwen et al., 2006).

1.5 Reactive oxygen species

Reactive oxygen species (ROS) are small, reactive molecules containing oxygen. These molecules are found within biological systems and their largest source is through formation as a byproduct of metabolism. There are various forms of ROS, which encompass both free radicals and molecular products. The origin however of all ROS produced though metabolic activity stem from the production of the anion radical form of molecular oxygen namely superoxide ($O_2^{\cdot -}$). Superoxide results from the premature univalent reduction of molecular oxygen by available electrons, which exit the ETC prior to their arrival at complex IV. Following the formation of $O_2^{\cdot -}$ it is the act of superoxide dismutase (SOD), which converts $O_2^{\cdot -}$ to hydrogen peroxide, a more stable form of ROS. Furthermore, subsequent redox sensitive reactions can result in the formation of other ROS such as hydroxyl radical through the Fenton reaction.

Mitochondria are a major source of cellular ROS. Most of the ROS in mitochondria are produced by the ETC, specifically at complexes I and III (Murphy, 2009). However, recent work has also established complex II (succinate dehydrogenase) as a site of ROS under certain electron transfer conditions (Quinlan et al., 2012). ROS production by mitochondria is inherently dependent on redox poise and the PMF across the MIM (Murphy, 2009). Due to the nature of O_2 its reduction occurs in a sequential fashion resulting in the transient formation of a singlet electron intermediate $O_2^{\cdot -}$. Electrons, liberated from the ETC, are responsible for the formation of $O_2^{\cdot -}$ independent of H_2O production. For example, a

hyperpolarized MIM (high PMF) leads to over-reduction of respiratory complexes, electron slippage (out of the ETC), and the univalent reduction of O_2 producing O_2^- (Murphy, 2009a).

Although ROS can be toxic at high concentrations, when maintained within tolerable limits they serve as important signaling molecules. Indeed, controlled ROS emission from mitochondria regulates a variety of processes, *e.g.,* increases in phosphorylation cascades by the inhibition of phosphatases including hypoxic signaling, insulin release, insulin sensitivity and adipocyte differentiation (Guzy and Schumacker, 2006; Li et al., 2012; Tormos et al., 2011). While some debate exists over the causal relationship, studies support a role for increase in ROS production leading to the development of insulin resistance, the hallmark of type 2 diabetes. In addition to the observed increase in ROS production during IR development the expression of mitochondrial targeted antioxidants show protective effects even in a high fat diet model (Houstis et al., 2006; Anderson et al., 2009).

For the most part, mitochondrial ROS production is elevated during State 4 respiration, a metabolic state in which the constituents of the ETC exist chiefly in their reduced forms (high PMF, low ATP demand). At complex I, $2e^-$ are accepted by FMN and passed via iron-sulfur clusters to ubiquinone (Q) resulting in reduction to ubiquinol (QH_2). Electron slippage at FMN or at the Q binding site may result in matrix $O_2^{\cdot -}$ production (Takeshige and Minakami, 1979; Pryde and Hirst, 2011; Murphy, 2009b; Hirst et al., 2008; Lambert and Brand, 2004b; Lambert and Brand, 2004). Additionally, the step-wise reduction of cytochrome c results in an increased chance for single electron reduction of O_2 by the $QH^{\cdot -}$ intermediate into both the matrix (Q_i) and the intermembrane space (Q_o) (Loschen et al., 1973; Murphy, 2009b; Muller et al., 2004) . Although the two major sites of mitochondrial

ROS production lay within complexes I and III there exists physiological relevance in other contributing sites of mitochondrial ROS. More recently complex II, succinate dehydrogenase, has been identified to liberate electrons during both forward and reverse electron transport (Quinlan et al., 2012b; Ralph et al., 2011). This contribution may become significant upon inhibition of complex I and/or III.

Other mitochondrial sites of $O_2^{\cdot -}$ production have been identified, though mechanistic insights remain lacking. The production at these sites depends on the specific substrates being oxidized and the metabolic state of the cell and include for example αKGDH, a TCA cycle enzyme, which produces $O_2^{\cdot -}$ in a process strongly dependent on the NADH/NAD^+ and αGPDH which donates electrons to Q, resulting in intermembrane space $O_2^{\cdot -}$ production (Adam-Vizi and Tretter, 2013; Zundorf et al., 2009; Starkov et al., 2004; Tretter and Adam-Vizi, 2004; Tretter et al., 2007). Another site of $O_2^{\cdot -}$ production is the ETF:QO site, which accepts electrons from β-oxidation during acyl-Co dehydrogenase activity at Q (Seifert et al., 2010; St-Pierre et al., 2002; Eaton, 2002). In addition dihydroorotate dehydrogenase, involved in pyrimidine biosynthesis, passes electrons to the Q pool for transport. The flavin site within the enzyme is a source for electron liberation (Forman and Kennedy, 1975; Lenaz, 2001). Other less widely recognized sites of $O_2^{\cdot -}$ production include P66shc, which is part of an enzymatic system that extracts electrons from the ETC specifically for the singlet reduction of O_2 to $O_2^{\cdot -}$ in the regulation of apoptosis (Giorgio et al., 2005). Mia40p and Erv1p are also potentially important sites of $O_2^{\cdot -}$ production as these protein import regulators are part of an intermembrane space redox pathway. Electrons are transferred from imported proteins to Erv1p via Mia40p in a procession of disulfide exchange reactions (Koehler et al., 2006; Mesecke et al., 2005).

To keep ROS levels in check, mitochondria are equipped with a series of anti-oxidative enzymes and low molecular weight molecules capable of quenching ROS. $O_2^{\cdot -}$ is dismutated in the matrix with high kinetics by superoxide dismutase-2 (SOD2) and in the cytoplasm by SOD1 to hydrogen peroxide (H_2O_2), a permeable form of ROS that is involved in many cell-signaling processes (Murphy, 2009). But H_2O_2 levels are also kept within tolerable limits via antioxidant systems, for example by glutathione (GSH)/glutathione peroxidase and peroxiredoxins. Of direct relevance to this thesis, the production of ROS by mitochondria can also be self-regulating with the activation and deactivation of proton leak through UCPs 2 and 3. Recently, it has been established that such a UCP2-dependent redox circuit is required for the control of glucose-stimulated insulin release from β cells in the pancreas (Mailloux et al., 2012).

Additional studies have shown that UCP3 facilitates the oxidation of fatty acids and mitigates ROS damage in muscle (Aguer et al., 2013; Harmancey et al., 2013; MacLellan et al., 2005; Gong et al., 2000a; Vidal-Puig et al., 2000). In particular, Harmancey *et al.,* (2013) showed that UCP3 was necessary in the heart for full oxidation of long chain fatty acids, whereas short chain fatty acid oxidation was normal.

1.6 Methods of ROS detection

Accurate measurement of cellular ROS levels has become a priority in various laboratories since ROS play important roles in signaling and disease. ROS detection methods have been mostly reliant on redox-active chemicals, such as AmplexRed, dihydro-dichlorofluorescein diacetate (H_2-DCFDA), dihydroethidium (DHE), and MitoSOX, which

react with different ROS to produce either a luminescent or fluorescent signal (Dikalov and Harrison, 2012). However, these chemicals display some unfavorable properties for quantification of ROS levels in a cell environment. For instance, H_2-DCFDA, a commonly employed sensor, non-specifically reacts with H_2O_2 and other ROS; can be reduced by redox active metals; and can also auto-catalyze ROS production (Dikalov and Harrison, 2012). Similarly, DHE and its mitochondrial targeted counterpart MitoSOX are commonly used in the detection of $O_2^{\cdot-}$. This method however has limitations in that oxidation of the sensor can form two products. While measurable 2-hydroxyethidium results from the reaction with $O_2^{\cdot-}$, ethidium can also be formed through non-specific redox reactions (Dikalov and Harrison, 2012). Since the spectra of these two products overlap it is not possible to accurately quantify $O_2^{\cdot-}$ production by the most commonly used fluorescence techniques. An additional problem associated with the used of these sensors is that they are irreversibly oxidized. Thus, while ROS production rates can be determined using these sensors, they are unable to detect dynamic fluctuations in ROS within cells.

Recently, focus has shifted to the use of redox-sensitive and ROS-sensitive fluorescent proteins that cycle between reduced and oxidized states based on their cellular environment. As a result, a change in the redox status of these probes modifies the physical conformation of the proteins, thereby altering their fluorescent output. Changes in fluorescence can then be translated into changes in redox status or ROS levels. As proteins, these new probes can be targeted to cell microenvironments and have been shown to display high sensitivity and specificity towards changes in redox status and cellular ROS levels.

Redox sensitive GFPs (roGFP) have more recently been engineered to yield accurate determinations of cellular redox status through ratiometric measurements, *i.e.*, they are monitored at two separate wavelengths (Gutscher et al., 2008; Belousov et al., 2006). As a result of this unique feature, measurements remain unaffected by potentially interfering parameters such as differences in expression level and changes in pH. While reduced roGFP2 is preferentially anionic, it becomes preferentially neutral when oxidized. The oxidation of this probe results in the formation of a C147-C204 disulfide bond, thereby introducing slight shifts in the neighboring residues relative to the chromophore and in the surrounding hydrogen bond network (Meyer and Dick, 2010). The observed conformational change consequently affects the observed fluorescence at the monitored wavelengths. Additionally, the compartmental targeting and enzymatic coupling (*e.g.*, with Grx1) introduces additional advantages in monitoring these redox changes (Meyer and Dick, 2010).

Likewise, the development of OxyR-YFP (HyPer), a reversible H_2O_2 biosensor has enabled researchers to detect dynamic fluctuations in H_2O_2 throughout the cell in a ratiometric manner (Belousov et al., 2006). This sensor consists of the insertion of cpYFP into the regulatory domain (RD) of the prokaryotic H_2O_2-sensing protein OxyR. In the presence of H_2O_2 reduced OxyR is oxidized at key cysteine residues C199 and C208, which reside in the regulatory domain. Oxidation at C199 results in the formation of a sulfenic acid and exposure from a hydrophobic pocket (Choi et al., 2001; Zheng et al., 1998). This reactive group then forms a disulfide bond with C208 and subsequently induces a dramatic conformational change in the OxyR-RD, thereby altering the fluorescence of the probe (Belousov et al., 2006).

On the other hand, pericam, a circularly permuted YFP biosensor originally containing a calmodulin-binding domain was thought to show high sensitivity and specificity to changes in Ca^{2+} within the cell. This ratiometric probe however, was recently recognized to detect fluctuations in $O_2^{\cdot -}$ in a non-ratiometric manner. For this reason the calmodulin-binding domain has been removed and the resultant probe, mitochondrial targeted circularly permuted YFP (mt-cpYFP), is used as a specific and sensitive probe for the detection of $O_2^{\cdot -}$ (Wang et al., 2008). All of these biosensors, being proteins, can be targeted to mitochondria and since they can cycle between reduced and oxidized forms they are capable of providing sensitive measurements for spatial and temporal changes in redox, H_2O_2 and $O_2^{\cdot -}$ respectively.

1.7 Mitochondrial superoxide flashes (mSOF)

Within the last five years mitochondrial ROS research has uncovered a new phenomenon referred to as mitochondrial superoxide flashes (mSOF) in which stochastic, quantal bursts of $O_2^{\cdot -}$ are produced on a quiescent background within a variety of cell types (Wang et al., 2008; Pouvreau, 2010; Wei et al., 2011; Fang et al., 2011). Intriguingly, all of such cell types express either UCP2 or UCP3. mt-cpYFP and tetramethylrhodamine, ethyl ester (TMRE), a cell-permeable, fluorescent dye taken-up into mitochondria based on mitochondrial membrane potential, have been used in the identification and study of mSOF and mitochondrial membrane potential, respectively (Fang et al., 2011; Ma et al., 2011; Pouvreau, 2010; Schwarzlander et al., 2012; Wei et al., 2011; Wang et al., 2008; Wei and Dirksen, 2012). While mitochondrial membrane depolarizations had previously been shown to occur naturally, these studies have shown, using confocal microscopy approaches, that mSOF occur together with depolarization events (Figure 2) (Wang et al., 2008; Pouvreau,

2010; Wei et al., 2011). Surprisingly, mSOF do not occur in all mitochondria within a given cell (Wang et al., 2008).

Experimental evidence unveiled that mSOF are metabolically linked events. Initial determinations showed their dependence on substrate availability with little to no flashes occurring in the absence of glucose (Wang et al., 2008). Additionally, proper functionality of the ETC, ATP synthase and the adenine nucleotide transporter (ANT) proved requisite, with many studies showing the abolition of flashes with the use of ETC inhibitors (Wei et al., 2011; Wang et al., 2008; Pouvreau, 2010; Fang et al., 2011). Finally, confirmation that superoxide is the cause of these events was based on three key findings: 1) SOD2 knockdown increases their frequency; 2) The presence of SOD mimetics, ROS scavengers and mitochondrial antioxidants decrease their frequency; and 3) Anoxia completely abolishes their existence (Wang et al., 2008; Huang et al., 2011). Likewise, MitoSOX fluorescence slowly increases over time suggesting that O_2^- production is present during observed mSOF (Huang et al., 2011).

Linked mitochondrial depolarization events are the result of the transient opening of a large transmembrane protein channel and were first identified in the context of mSOF through loss of Rhod-2 fluorescence, due to mitochondrial Ca^{2+} binding (Wang et al., 2008). Additional findings supporting this claim showed mitochondrial swelling over the duration of these events (Ma et al., 2011; Wang et al., 2008). Conflicting evidence exists however, as to the identity of the large transmembrane protein channel, which is linked to these events and ultimately may play a role in the regulation of mSOF (Wang et al., 2008; Pouvreau, 2010).

Figure 2

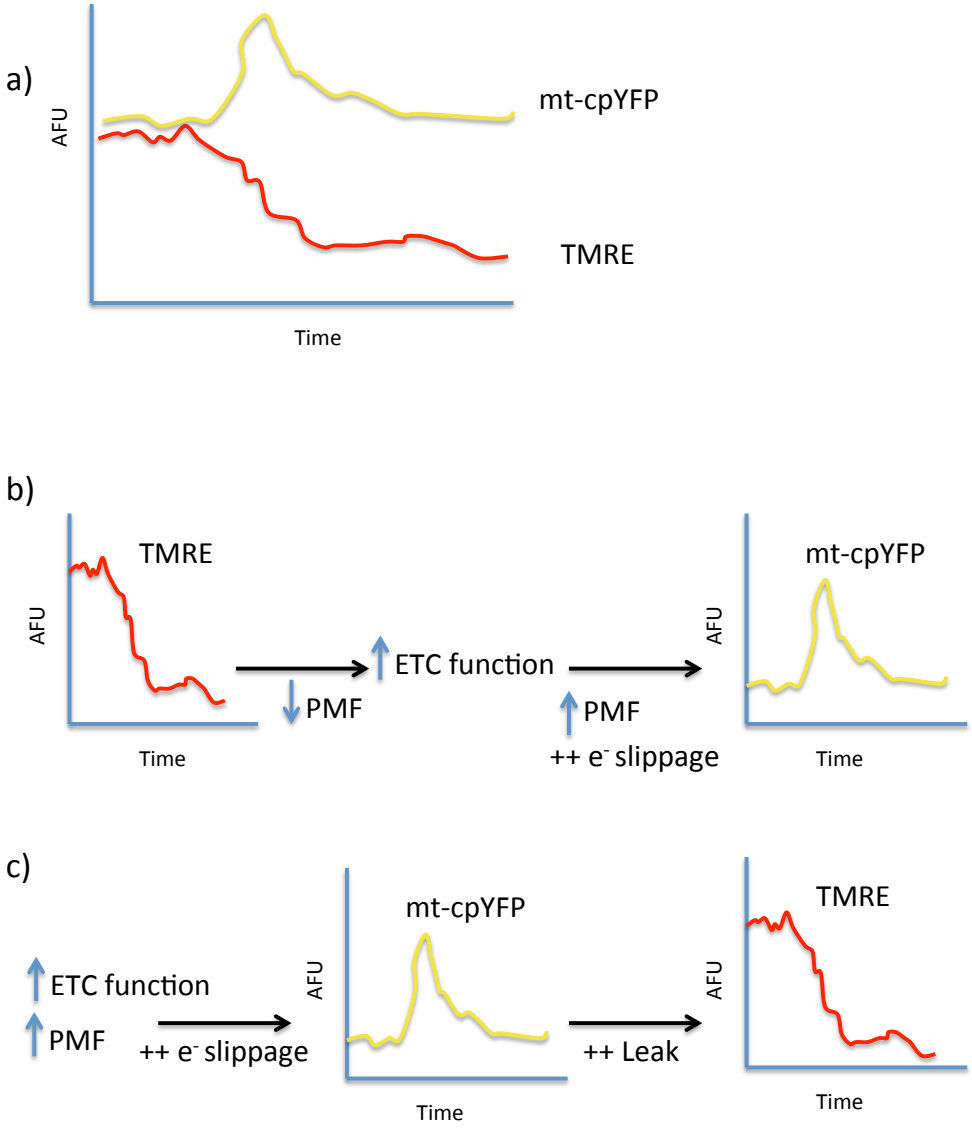
a)
AFU
mt-cpYFP
TMRE
Time
b)
AFU
TMRE
Time
PMF
ETC function
PMF
++ e- slippage
AFU
mt-cpYFP
Time
c)
ETC function
PMF
++ e- slippage
AFU
mt-cpYFP
Time
++ Leak
AFU
TMRE
Time

Figure 2- mSOF event profile and two potential mechanisms for mSOF generation.a) Example trace of mSOF event monitored with a superoxide sensitive biosensor, mt-cpYFP (yellow), and a mitochondrial membrane potential dye, TMRE (Red). Two potential mechanisms outlining the temporal series of events governing mSOF events b) Pore opening (leak mechanisms) trigger mSOF events. Leak mechanisms are activated by slight hyperpolarization in MIM and constitutive ROS production causing membrane depolarizations (decreased TMRE signal). Subsequently the ETC is stimulated to restore the PMF through increased ETC function. These increases in ETC function increase the PMF and additionally cause increased electron (e^-) slippage (as PMFgradually increases), resulting in a burst of superoxide ($O_2^{-\cdot}$) production visualized as peak in mt-cpYFP fluoresence. c) Pore opening (leak mechanisms) turns off mSOF. Increases in ETC function result in slight hyperpolarization of the MIM. Hyperpolarization of the MIM causes increased electron slippage resulting in mSOF. Activation of leak mechanisms as a result of increased superoxide production results in the depolarization of the MIM.

Initially, involvement of the mitochondrial permeability transition pore (mPTP), well known for its activation by ROS, was elucidated through flash abolition in the presence of mPTP inhibitors (carboxyatractyloside and bongkrekic acid) (Wang et al., 2008). Additional findings by Pouvreau *et al*. however, showed that mSOF remain unaffected under the same conditions (Pouvreau, 2010). Through use of inhibitors of the inner membrane anion channel (IMAC) a role for this transmembrane protein in regulating mSOF was dismissed (Pouvreau, 2010). Although flashes are linked to depolarization events, membrane depolarizations are also observed in the absence of mSOF. The latter is important in the context of the possible regulatory mechanisms (Figure 2b&c) (Wang et al., 2008; Pouvreau, 2010; Wei et al., 2011).

The relevance of mSOF in the context of the cell and cellular processes remains to be determined. In order to understand their relevance it is first important to fully characterize the events. Still unknown are the transmembrane protein(s) responsible for governing the depolarization events; the associated regulatory mechanisms, and the mechanistic details of these events.

2.0 OVERALL AIM, RATIONALE, HYPOTHESIS AND RESEARCH OBJECTIVES:

2.1 Overall Aim:

The **overall aim of my project** is to establish methods to investigate the characteristics and mechanistic details governing mSOF in skeletal muscle.

2.2 Rationale and Hypotheses:

Given the limited but well-established evidence in the literature for the existence of temporally linked mitochondrial depolarizations and mSOF, we hypothesize that UCP3, as a

MIM transmembrane protein involved in a membrane-depolarizing proton leak activated by ROS, is involved to some extent in controlling the occurrence and characteristics of mSOF in skeletal muscle cells. Additionally, it is expected that through the use of spinning disk confocal imaging technology the discernment of temporally linked characteristics of mSOF, will shed light overall on the mechanisms controlling mitochondrial ROS emission. Finally, an exploratory study utilizing mouse myofiber preparations will further our understanding of the homogeneity or heterogeneity of flash characteristics among skeletal muscles with various fiber type compositions.

2.3 Research Objectives:

1. To propagate mito-Grx1-roGFP2 and cyto-Grx1-roGFP2 redox sensitive and pHyPer-dmito hydrogen peroxide sensitive biosensors.
2. To assess the appropriateness of pHyPer-dmito as a sensor for mSOF determinations.
3. To determine the contribution of UCP3 in the regulation of mSOF events using mt-cpYFP.
4. To determine the relationship between mSOF events and depolarization.
5. To identify characteristics of mSOF events in isolated myofibers from various muscles.

3.0 MATERIALS AND METHODS:

3.1 Plasmid Preparation:

Plasmid DNA encoding biosensors mitochondrial targeted glutaredoxin conjugated redox sensitive GFP (mito-Grx1-roGFP2), cytosol targeted glutaredoxin conjugated redox sensitive GFP (cyto-Grx1-roGFP2) (a generous gift of Dr. Tobias Dick; DKFZ, Heidelberg, Germany) (Meyer and Dick, 2010b), Mitochondrial targeted hydrogen peroxide sensitive YFP (pHyPer-dmito) (Evrogen, Moscow, Russia) (Belousov et al., 2006) and mitochondrial targeted circularly permuted superoxide sensitive YFP (mt-cpYFP) (a generous gift of Dr. Robert Dirksen; University of Rochester, Rochester, NY) (Wang et al., 2008) were propagated in a bacterial system for isolation. Plasmid DNA was diluted 10x and mixed 1:9 (v:v) with chemically competent DH5α cells (Invitrogen, Burlington, ON) and incubated 30 min at 4 ^{o}C. Transformation was carried out by heat shock exposure performed for 90 s at 42 ^{o}C, which was immediately followed by the addition of 500 µL S.O.C. medium (2% tryptone, 0.5% yeast extract, 10 mM NaCl, 2.5 mM KCl, 10 mM $MgCl_2$, 10 mM $MgSO_4$, and 20 mM glucose) (Invitrogen, Burlington, ON) and incubated 1h 37 ^{o}C, ~250 rpm. Following incubation, 100 µL of the transformation reaction was plated on sterile lysogeny broth (LB) Miller agar plates (171 mM NaCl, 10 g/L tryptone, 5 g/L yeast extract and 20 g/L agar, pH 7.0) ±antibiotics (100 mg/L ampicillin or 2.5 µg/mL kanamycin) and left to incubate at 37 ^{o}C for 24 h.

Following transformation, colonies were selected from LB-Miller agar plates containing antibiotic selection and grown in a 5 mL culture in sterile NZY+ broth (10 g/L NZ amine casein hydrolysate, 5 g/L yeast extract, 85.5 mM NaCl, 12.5 mM $MgCl_2$, 12.5 mM $MgSO_4$ and 0.4% (w/v) D-glucose, pH 7.5) with antibiotic selection (100 mg/L ampicillin or

2.5 µg/mL kanamycin) at 37 ^{o}C, 6 h, ~250 rpm. Day cultures were transferred to 200 mL overnight cultures grown under the same conditions. Plasmid DNA was purified from overnight cultures using the PureYield Plasmid Maxiprep system (Promega, Madison, WI). Bacterial cells were pelleted by centrifugation using a high speed centrifuge with a JA-25.50 fixed angle rotor (Avanti J2-21M; Beckman Coulter, Mississauga, ON) for 10 min at 5000 xg and resuspended in 12 mL resuspension solution. Cell lysis was accomplished with the addition of 12 mL of cell lysis solution followed by inversion and 3 min incubation at room temperature (RT). The lysis reaction was terminated with the addition of 12 mL of neutralization solution to the lysate. Cellular debris was removed from the resulting lysate by centrifugation with a high-speed centrifuge with a JA-25.50 fixed angle rotor (Avanti J2-21M; Beckman Coulter, Mississauga, ON) for 20 min at 14000 xg.

Purification of DNA was achieved by passing lysate through the PureYield clearing column and PureYield Maxi binding column with application of a vacuum. Endotoxins were removed by washing the column with 5 mL of an endotoxin removal solution and subsequently the column was washed with 20mL of column wash solution. Column-bound plasmid DNA was eluted with nuclease-free water by centrifugation using a swinging bucket rotor (Sorvall ST-16TR; Thermo Scientific, Waltham, MA) at 2000 xg for 5 min. Final concentration of purified plasmid were determined using the NanoDrop 2000 UV-Vis spectrophotometer (Thermo Scientific, Waltham, MA).

Following isolation, plasmid identity was confirmed via restriction enzyme detection. 1µg of plasmid DNA was introduced into a 50 µL reaction containing 1 µL of two unique restriction enzymes (*Bgl*II, *Cla*I, *Hpa*I, *BamH*I, *Hind*III, *Kpn*I) and the appropriate reaction

buffer (New England Biolabs, Whitby, ON) for 1 h at 37 ^{o}C. Products of the restriction enzyme digest reaction were run alongside 100 bp and 1 kb GeneRuler DNA ladders (Fisher Scientific, Waltham, MA) on a 0.8% agarose gel in TAE buffer (40 nM Tris, 20 mM glacial acetic acid, 1 mM EDTA), 1 h at 80 V, for visualization with ethidium bromide. Plasmid DNA identity was confirmed by comparing observed DNA fragment sizes to the theoretical expected size of restriction enzyme products (Figure 3).

3.2 Cell Culture:

Chinese Hamster Ovary (CHO) and Human Embryonic Kidney (HEK) 293 (ATCC, Manassas, VA) derived cell lines were cultured on Matrigel (BD Biosciences, Franklin Lakes, NJ) coated culture flasks in Dulbecco's modified Eagles' medium (DMEM) (Gibco, 11995-065, Burlington, ON) supplemented with 20% FBS and 2% antimycotics-antibiotics (AA). Cells were kept in a temperature- and gas-controlled Revco Ultima incubator (GS Laboratory Equipment, Asheville, NC) (37 ^{o}C, 5% CO_2). For experiments cells, were lifted enzymatically with trypsin-EDTA.

3.3 Transient Transfections:

Cells were seeded 50,000 cells/mL and grown to ~80% confluency. Propagated plasmid DNA (mito-Grx1-roGFP2, cyto-Grx1-roGFP2 or pHyPer-dmito) diluted in DMEM (in the absence of FBS and AA) was mixed with Lipofectamine 2000 (Invitrogen, Burlington, ON) based on recommended treatment volumes and incubated 20 min, at RT. Following incubation medium was removed from cells and replaced with Lipofectamine/DNA complex and medium (no AA) was added. 24 h post transfection, cells were collected or treated for experimental uses accordingly.

Figure 3

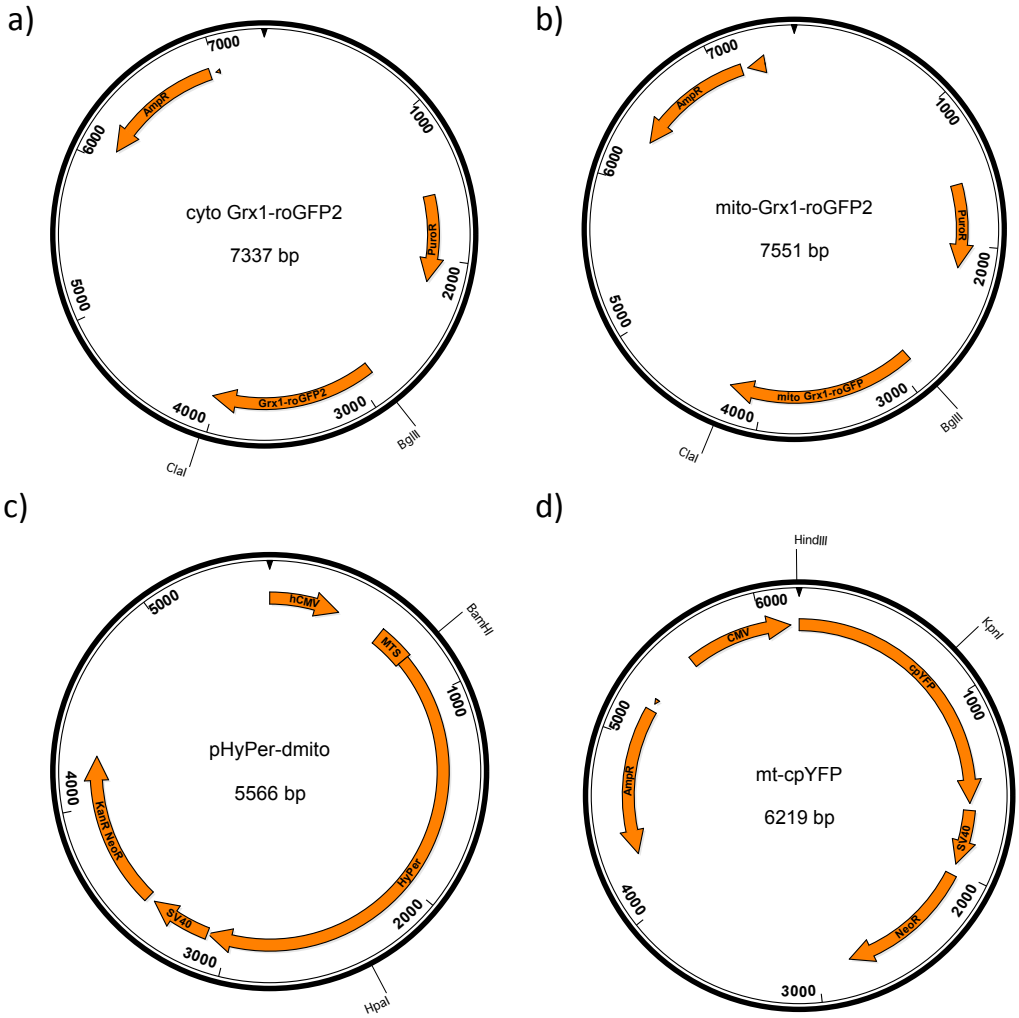
a)
cyto Grx1-roGFP2
7337 bp
AmpR
PuroR
Grx1-roGFP2
ClaI
BglII
b)
mito-Grx1-roGFP2
7551 bp
AmpR
PuroR
mito Grx1-roGFP
ClaI
BglII
c)
pHyPer-dmito
5566 bp
hCMV
MTS
HyPer
SV40
KanR NeoR
BamHI
HpaI
d)
mt-cpYFP
6219 bp
CMV
cpYFP
SV40
AmpR
NeoR
HindIII
KpnI

Figure 3- Fluorescent protein biosensor expression constructs. Plasmid maps outlining promoters, protein biosensor gene location, resistance genes and pertinent restriction enzyme cut sites. a) Cyto-Grx1-roGFP2 b) mito-Grx1-roGFP2 c) pHyper-dmito and d) mt-cpYFP.

3.4 Cellular Lysis and Tissue Homogenization:

Cellular lysis and tissue homogenization for immunoblotting was carried out in radio-immunoprecipitation assay buffer (RIPA; 50 mM Tris, 150 mM NaCl, 0.1% w/v SDS, 0.5% sodium deoxycholate, 1.0% NP-40 and 1X Protease Inhibitor Cocktail added fresh). Cells were lysed (10 min, 4 ^{o}C) and tissue was homogenized using an ice-cold glass/Teflon Potter-Elvehjem tissue grinder three times for 20 passes with remaining whole cells being removed from both lysates via centrifugation (150 xg, 10 min, 4 ^{o}C) using an IEC Micromax RF centrifuge (Harlow Scientific, Arlington, MA). Total cellular protein was determined using the Bicinchoninic Acid (BCA) Assay. Samples were diluted and run alongside standards of known bovine serum albumin (BSA) concentrations (Sigma, Mississauga, ON) incubated 1:1 (v/v) with BCA working reagent (Reagent A: 0.645 M $NaHCO_3$, 69.5 mM sodium tartrate, pH 11.25; Reagent B: 0.103 M BCA; Reagent C: 0.16 M copper sulphate, mixed 26:25:1 (v/v/v), respectively) (65 ^{o}C, 30 min). The absorbance at 562 nm was read for each standard and sample using the Synergy Mx2 microplate reader and Gen5 software (BioTek; Winooski, VT) and a standard curve was constructed to determine the relative protein concentrations of the samples.

Cellular homogenization for cell free extract experiments was carried out in isolation buffer (220 mM mannitol, 70 mM sucrose, 5 mM HEPES and 1 mM EGTA, pH 7.2). Cells were collected, resuspended in ice-cold homogenization buffer and homogenized as above. Homogenate was cleared of whole cells and nuclei by centrifugation (800 xg, 5 min, 4 ^{o}C) using an IEC Micromax RF centrifuge (Harlow Scientific, Arlington, MA). Total homogenate protein was determined using the Bradford assay whereby samples were diluted and run along side standards of known BSA concentrations (Sigma, Mississauga, ON)

incubated 1:4 with Bradford reagent (BioRad Laboratories, Hercules, CA). The absorbance at 595 nm was read for each standard and sample using the Synergy Mx2 microplate reader and Gen5 software (BioTek; Winooski, VT) and a standard curve was constructed to determine relative protein concentrations of the samples.

3.5 SDS-PAGE and Immunoblotting:

Protein samples were diluted with lysis buffer and 5X loading buffer (0.3125 M Tris-HCl pH 6.8, 50% glycerol, 10% SDS, 0.05% bromophenol blue 12.5% β-mercaptoethanol) to a final concentration of 2 μg/μL and heated (95 ^{o}C, 5 min) prior to loading on the denaturing discontinuous polyacrylamide gel. Resolving gel (10%) and stacking gel (4%) were prepared (10% acrylamide/bisacrylamide 29:1, 0.375 M Tris-base (pH 8.8), 0.1% SDS) and (4% acrylamide/bisacrylamide 29:1, 0.125 M Tris-base (pH 6.8), 0.1% SDS), respectively, and polymerized with 0.6% ammonium persulfate (APS) and 20 μL N,N,N',N'-tetramethylethane-1,2-diamine (TEMED). Briefly, resolving gel was poured and overlaid with 100% isopropanol. Once polymerized, the isopropanol was removed, the stacking gel was poured, a 1.5 mm well comb inserted and the gel was allowed to polymerize. Polymerized gels were placed in the mini-PROTEAN electrophoresis unit (BioRad; Mississauga, ON) and unit was filled with SDS-PAGE running buffer (25 mM Tris-base, 192 mM glycine, 0.1% w/v SDS). Aliquots of ladder proteins (PageRuler prestained protein ladder; Pierce Biotechnology, Rockford, IL) and equal protein-containing samples were loaded and electrophoresed at a constant voltage of 100 V. Gels were set up for protein transfer once the dye front had reached the end of the gel.

A transfer sandwich was constructed consisting of two sponge fiber pads, four filter papers, one gel and one nitrocellulose membrane and placed in the Mini-Protean tetra cell transfer apparatus (BioRad; Mississauga, ON). Transfer was conducted at 100 V for 1 h in transfer buffer (20% methanol, 50 mM Tris-base, 38 mM glycine, 0.1% SDS) under constant stirring and in the presence of a block of ice.

Following protein transfer, membranes were blocked with 5% w/v skim milk in Tris-buffered saline containing 1% v/v Tween-20 (TBS-T) for 1 h at RT. Blots were rinsed and washed three times for 5min with TBS-T and subsequently probed overnight 4 ^{o}C with primary antibody for the protein of interest. Primary antibodies included: goat polyclonal anti-UCP2 (N-19) antibody (1:500 5% w/v milk; Santa Cruz Biotechnology, Santa Cruz, CA); rabbit polyclonal anti-Tag (CGY)FP antibody (1:5000 TBS-T; Evrogen, Moscow, Russia); rabbit polyclonal anti-GFP antibody (1:1000 TBS-T; Abcam, Cambridge, MA); mouse monoclonal anti-α-tubulin antibody (1:5000 5% w/v milk; Sigma, St. Louis, MO); rabbit polyclonal anti-succinate dehydrogenase (SDHA) antibody (1:2000 5% w/v milk; Santa Cruz Biotechnology, Santa Cruz, CA); and rabbit polyclonal anti-SOD2 (FL-222) antibody (1:2000 TBS-T; Santa Cruz Biotechnology, Santa Cruz, CA). Blots were then washed and probed with the appropriate horseradish peroxidase conjugated secondary antibody for 1 h, at RT in 5% w/v skim milk in TBS-T. Secondary antibodies included: goat anti-mouse IgG-HRP; goat anti-rabbit IgG-HRP; and donkey anti-goat IgG-HRP), and were purchased from Santa Cruz Biotechnology, Santa Cruz, CA. Secondary antibodies were incubated at 1:2000 5% w/v milk for 1 h, at RT, except for the secondary antibody to α-tubulin, which was probed 1:4000 in 5% w/v milk for 1 h at RT. Finally, membranes were rinsed washed three times for 5min with TBS-T and exposed to enhanced chemiluminescent

substrate (ECL kit; Thermo-Fisher Scientific, Waltham, MA) for 2 min prior to conducting film exposure in a dark room.

3.6 Bioenergetic Measurements:

Assessments of mitochondrial bioenergetics of CHOEV and CHOUCP3 cells were carried out using the Seahorse XF24 analyzer (Seahorse Biosciences, North Billerica, MA). The Seahorse XF24 analyzer creates a 7 μL microenvironment by lowering its fluorescent probes 200 μm above the biological sample adhered in the wells of the in the 24 well assay plate (Ferrick et al., 2008). This method allows real-time fluorescent probe monitoring of oxygen consumption rates (OCR) and extracellular acidification rates (ECAR) in intact cells. Measurements of OCR within the assay medium reflect aerobic respiration since the O_2 in the assay medium is consumed by its cellular reduction to H_2O by the electron transport chain. Similarly, ECAR is a proxy measure of glycolysis since the acidification of the medium is due largely to cellular release of lactic acid, an end-product of glycolysis.

First, cells were plated (25,000 cells/well) in Matrigel coated 24-well XF24 Seahorse assay plates (Seahorse Biosciences, North Billerica, MA) and incubated overnight (37 ^{o}C, 5% CO_2) to adhere. Cells were placed in XF assay medium (DMEM, 4 mM L-glutamine, 1 mM sodium pyruvate ± 25 mM glucose) for 30 min while probes were calibrated. OCR and ECAR were measured simultaneously throughout the following protocol. Three measurements of resting respiration were made with each measurement interval consisting of 2 min mixing, 2 min incubation and 2 min measurement steps. Subsequent inhibition of ATP synthase by the addition of 2 μg/mL oligomycin enabled assessment of state 4_o respiration and glycolytic capacity across two measurement intervals. Addition of 1.5 μM of the

chemical uncoupler, carbonyl cyanide 4-(trifluoromethoxy)phenlyhydrazone (FCCP) followed by two measurement intervals allowed the assessment of maximal respiratory capacity of the cells. Finally, the addition of 2.3 μM antimycin A (Ant A), an inhibitor of electron transfer in Complex III, followed by two measurement intervals allowed for the evaluation of any extramitochondrial OCR.

3.7 Flow Cytometry and Fluorescence Activated Cell Sorting (FACS):

Cells were washed with Hank's Balanced Salt Solution (HBSS), lifted enzymatically with trypsin-EDTA, resuspended as a single cell suspension in HBSS (~100 μL/200,000 cells) and fixed in 1% paraformaldehyde (PFA). Prior to data acquisition fixed samples were diluted in an isotonic solution (Beckman Coulter, Mississauga, ON) and vortexed. Data was acquired using the Cyan ADP 9 analyzer (Beckman Coulter, Mississauga, ON) and Summit v4.3 Software (Dako, Burlington, ON). Events were collected with excitation using either a 405 nm or 488 nm solid-state laser and sample fluorescence was detected with a gain of 1 through one of three bandpass filters (FITC; dichroic 545 nmLP, 530 nm/40, 410 V, Violet 1; dichroic 485 nmLP, 450 nm/50, 441 V or Violet 2; dichroic 485 nmLP, 430 nm/40, 472 V). Data analysis was carried out using Kaluza Analysis Software 1.2 (Beckman Coulter, Mississauga, ON). Live cells were identified and gated based on forward scatter (FSC) and side scatter (SSC) plots.

Cells were prepared for FACS as above without fixation or dilution. FACS was carried out using MoFlo XDP (Beckman Coulter, Mississauga, ON) and Summit v4.3 Software (Dako, Burlington, ON). Events were recorded with excitation by a coherent

sapphire 488 nm laser with detection in the YFP channel (FL1; Dichroic 505 nmSP, 530 nm/40, 423 V)

3.8 Stable Cell Line Development:

To establish kill curves for the determination of antibiotic selection concentration, HEK293 cells were plated 25,000 cells/mL and left to undergo one round of cell division. Then HEK293 cells were treated with selection media containing increasing amounts of antibiotics (Geneticin or Puromycin). A 3-(4,5-dimethylthiazol-2-yl)-2,5-diphenyltetrazolium bromide (MTT) assay was performed each day for 5 d to assess the cell viability compared to the untreated control. For the MTT assay, selection medium was removed and replaced with 100 µL of fresh culture medium and 10 µL MTT reagent. Cells were incubated under normal cell culture conditions for 1.5 h after which time media containing MTT was removed and cells were lysed and formazan solubilized in 100µL isopropanol containing 0.04 N HCl and the absorbance was read at 570 nm with reference taken at 630 nm using the Synergy Mx microplate reader and Gen5 software (BioTek; Winooski, VT).

Following selection of an appropriate concentration of antibiotic for selection, HEK293 cells were plated and transfected as mentioned above. 24 h post transfection appropriate selection medium was added to transfected cultures. Cell cultures were monitored, changing selection media every 2-3 d until no live cells remained in the untransfected control exposed to selection, ~10 d. Stably expressing cell lines were maintained in half of the antibiotic concentration used during selection. Expressing populations were assessed on a Zeiss AxioObserver.D1 inverted microscope and AxioVision

4.8 software (Carl Zeiss, Oberkochen, Germany) using a 20x (LD Plan-NeoFluar 0.4 Corr Ph1 Ph2) objective with transmitted light and excitation by a FluorArc Mercury Lamp using Zeiss filter set 46 (Ex BP 500 nm/25, BS FT 515 nm, Em BP 535 nm/30).

3.9 Microscopic assessments of roGFPs and p-HyPer-dmito:

Co-localization of cyto-Grx1-roGFP2 and mito-Grx1-roGFP2 expression in transiently transfected CHOEV cells was assessed using a Leica Spinning Disk Confocal microscope, BMI600B (Leica; Wetzlar, Germany) controlled by Volocity 3D Image Analysis Software (PerkinElmer, Waltham, MA). Cells were transfected as outlined above with cyto-Grx1-roGFP2 or mito-Grx1-roGFP2 and exposed to 20 nM TMRE for 20 min prior to imaging with a Leica 63x oil immersion objective (NA 1.4). Cells expressing roGFPs and containing TMRE dye were excited with 406 nm and 561 nm laser lines and detected with 525 nm/36 and 605 nm/52 filters, respectively. Localization was assessed using the dual channel overlay function and the Pearson's correlation coefficient on Volocity software (PerkinElmer, Waltham, MA).

Preliminary assessments of the responsiveness of pHyPer-dmito in intact cells to the addition of H_2O_2 were performed on a wide-field deconvolution based DeltaVision CORE microscope equipped with a three-dimensional motorized stage, temperature-and gas-controlled environmental chamber, Xenon light source, and a quantifiable laser module controlled by SoftWorX acquisition and deconvolution software (Applied Precision, Issaquah, WA). Stably transfected pHyPer-dmito expressing HEK293 cells were monitored with a 60x (NA 1.4) objective with excitation using a 488 nm laser and emission 528 nm/38 at a rate of 2 frames/min with the sequential addition of exogenous H_2O_2 over time.

3.10 Characterization of pHyPer-dmito using a microplate reader:

For determinations made in intact cells, cells were plated and treated accordingly in a 96-well clear-bottom black-sided microplate such that they reached confluency for experiments. For determinations made in a cell-free extract system, cell-free extract samples were diluted to 0.3 µg/µL in reaction buffer (isolation buffer + 5 mM $MgCl_2$, 10 mM KH_2PO_4, 0.2% w/v BSA and 2 mM DTT) and 45 µg protein/well was used for determinations. Sensitivity, reversibility and kinetic determinations were carried out on a Synergy Mx2 microplate reader controlled by Gen5 software (BioTek; Winooski, VT). Fluorescence of pHyPer-dmito expressing samples were excited with 420 nm and 488 nm light and monitored for fluorescent emissions at 515 nm every 10-21 s throughout the experiment. Additions of exogenous H_2O_2 and DTT were controlled via the injection ports equipped on the microplate reader. The ratio between the emissions at each of these wavelengths was calculated and expressed relative to the first read (set ratio=1).

3.11 Mice:

C57BL/6J WT and whole body UCP3 knockout (C57BL/6J genetic background) mice were used for the initial determinations of mSOF. WT mice were originally acquired from the Jackson Laboratory (Jackson Laboratory; Bar Harbor, ME) and breeding colony was established in the Faculty of Medicine. UCP3KO mice were generated as previously described (Gong et al., 2000). mt-cpYFP skeletal muscle specific transgenic mice backcrossed onto a C57BL/6N background were acquired from collaborators (Dr. Robert Dirksen; University of Rochester, NY). All experiments were approved by the Animal Care Committee at the University of Ottawa in accordance with the guidelines of the Canadian

Council of Animal Care or the University of Rochester Committee of Animal Resources. All mice were housed in a temperature- and light- controlled environment (23^{o}C; light 6:00-18:00) with free access to a standard chow diet (44.2% carbohydrate, 6.2% fat and 18.6% crude protein (Harlan Laboratories, Mississauga, ON) and water.

3.12 Electroporation of mt-cpYFP:

Hind limb foot pads of WT and UCP3KO mice were electroporated with mt-cpYFP to facilitate visualization of mSOF in muscle fibers. Mice were injected interperitoneally with 10μL anesthetic /10 g body weight. The anesthetic was 10 mg/mL ketamine, 1 mg/mL xylazine and 0.3 mg/mL acepromazine, and anesthesia was confirmed with a footpad pinch. Subsequently, bovine hyaluronidase (8 μL of 2 μg/μL) was injected subcutaneously into each hind limb footpad, massaged and then left for 1 h to allow digestion of extracellular matrix proteins. The foodpad pinch test was repeated to ensure that anesthetization was maintained prior to the injection of 15 μL of 2 μg/μL mt-cpYFP cDNA in 71 mM NaCl. Electroporation was accomplished 10 min later with 100 V/cm delivered for 20 ms at a rate of 1 Hz for 20 pulses using subcutaneous gold-plated electrode placed perpendicularly to the long axis of the muscle, close to the proximal and distal tendons. Mice were monitored for recovery from anesthetic and returned to their original housing. Experiments using electroporated mice were performed one wk post electroporation.

3.13 mSOF determinations:

One wk post electroporation or on the day of the experiment in WT or UCP3KO mice, flexor digitorum brevis (FDB) muscle was dissected out of each hind limb footpad and single muscle fibers were isolated by enzymatic dissociation with 1-1.2 mg/mL collagenase

A (37^{o}C, 45 min-1 h) in regular rodent Ringer's solution (RRR) (146 mM NaCl, 5 mM KCl, 2 mM $MgCl_2$ 2 mM $CaCl_2$ and 10 mM HEPES, pH 7.4). Following dissociation single fibers were plated in 35-mm glass-bottom dishes (MatTek, Ashland, MA) and left for 30 min to ensure adhesion prior to the addition of FDB culture medium (1:1 DMEM/F12, 2%FBS, 1% penicillin/streptomycin) and kept in an incubator (37 ^{o}C, 5% CO_2) until used. Fibers were kept in a 1:1 (v/v) DMEM/F12 medium (Life Technologies, Burlington, ON) until imaging and all fibers were used the day of isolation.

At the time of microscopy, culture medium was removed and an imaging medium (RRR supplemented with 5 mM glucose) containing 20 nM TMRE was added to the fibers in the dark at least 10 min prior to imaging. mSOF events were imaged using a Nikon Eclipse C1 Plus confocal microscope and EZ C1 software (Nikon Instruments, Melville, NY). Mt-cpYFP and TMRE were excited using 488 nm (x8-16 attenuation) and 543 nm (x64 attenuation) lasers and detected at 515 nm/30 and 605 nm/75 emission respectively. Using a SuperFluor 40x (NA 1.3) oil immersion objective 100 frames of time-lapse x,y images were obtained at a rate of 1.24 s/frame and a resolution of 512 x 512 pixels.

Determinations for muscle specific mSOF comparisons and temporal resolution of events were carried out using mice having transgenic expression of mt-cpYFP under the control of the human α-skeletal actin (HAS) promoter. Briefly, *in situ* differentiated myotybes were isolated from FDB, Soleus and extensor digitorum longus (EDL) as previously described and plated into imaging chambers (ibidi; Martinsried, Germany). Imaging was carried out on a Leica Spinning Disk Confocal microscope, BMI600B (Leica; Wetzlar, Germany) controlled by Metamorph software. Mt-cpYFP and TMRE were excited

using 490nm and 561nm lasers and detected using a 525/36 nm and 605/52 nm bandpass emission filters, respectively. Using a PL APO 40x (NA 1.3) oil immersion objective 125 frames of time-lapse x,y images were obtained at a rate of 1 s/frame and a resolution of 512x512 pixels.

3.14 mSOF analysis:

Images acquired were pre-processed using Image J software (NIH, USA) by first aligning all photos from the time lapse using the register region of interest (ROI) function and adjusting the image file type to an 8-bit image. Pre-processed images were then subjected to automated detection and analysis of mSOF using a MATLAB-based command line prompt program called 'Flash Collector' (University of Rochester, Rochester, NY), which identifies and quantifies a number of flash parameters including flash frequency, amplitude, duration, full duration at half maximum (FDHM), decay constant (τ), time to peak and spatial area from the time lapse image series. To do this, the program calculated the standard deviation (SD) for each pixel in the time series; those with standard deviations >37-65% of the maximum standard deviation were used to select ROIs for further processing. Regions with areas smaller than 5 pixels were subsequently discarded and the analysis was further refined using the following criteria: minimum threshold of maximum intensity of mean + (2.8-3.4) x standard deviation, flash decay described by a single exponential decay function with fitting error <10 and a minimum amplitude ($\Delta F/F_o$) of 0.2. Strict universal parameters were maintained for analysis of transgenic expressing mt-cpYFP animals (% standard deviation to start=22 and standard multiplier=3.0).

Additional analysis of changes in TMRE fluorescence was carried out manually using ImageJ by selecting a ROI and using the measure function on all images from the stack. Subsequent analyses and comparisons on collected data were facilitated using R software (Freeware; University of Auckland, Auckland, New Zealand) to sort and organize the requisite data from that collected.

3.16 Electron microscopy

FDB was dissected out of the hind limb footpad, fixed (2.5% glutaraldehyde, 2% PFA in PBS, pH 7.4) and stored at 4^{o}C before imaging. Muscle was embedded in LR white (Marivac) and thin sections were cut with a Leica Ultracut E ultramicrotome. Sections were counterstained with lead citrate and uranyl acetate and digital images were taken using a JEOL 1230 transmission electron microscope at 60 kV adapted with a 2 × 2 K bottom-mount CCD digital camera (Hamamatsu) and AMT software. Subsequently, mitochondrial areas were measured in ImageJ and tabulated.

3.15 Statistics:

Statistical analyses were performed using GraphPad Prism v6.0d (GraphPad Software, San Diego, CA). For normally distributed data a Student's t-test was performed for two mean comparisons. Additionally, a Mann-Whitney test was performed for data that were not normally distributed. All tests were conducted with values of $p<0.05$ considered statistically significant. Data are presented as mean ± SEM.

4.0 RESULTS:

4.1 Propagation of redox sensitive and hydrogen peroxide fluorescent biosensors and development of model system

The mitochondrion, heavily relied on for the production of cellular ATP, depends on a complex series of redox reactions, including those in the ETC. The mitochondrial environment is subject to fluctuations in redox status during fuel oxidation, electron transfer and also during the formation of ROS. Many mitochondrial processes and enzymatic reactions are dependent on the redox status of the matrix. Thus we sought to investigate mSOF as they related to changes observed in redox within the mitochondria.

To begin, two redox sensitive GFP probes, Mito-Grx1-roGFP2 and Cyto-Grx1-roGFP2, were chosen. Probe DNA was propagated and their identity was confirmed (Figure 4a). Similarly, a model system, Chinese Hamster Ovary (CHO) cells, which stably expressed either an empty vector (CHOEV) or uncoupling protein 3 (CHOUCP3) was chosen. Transient transfection conditions were optimized in the model system with Western blot detection for GFP (Figure 4b). These optimized conditions were then used in preliminary experiments conducted using a Leica spinning disk confocal microscope. Probes were tested for proper localization: mitochondrial or cytosolic, by assessing their co-localization with TMRE (Figure 4c&d).

Bioenergetic measurements of CHOEV and CHOUCP3 cells were carried out in order to characterize the metabolism of TCA cycle substrates in the presence or absence of glucose. It was noted that CHOEV cells were more glycolytic (*i.e.*, had higher ECAR) than

Figure 4

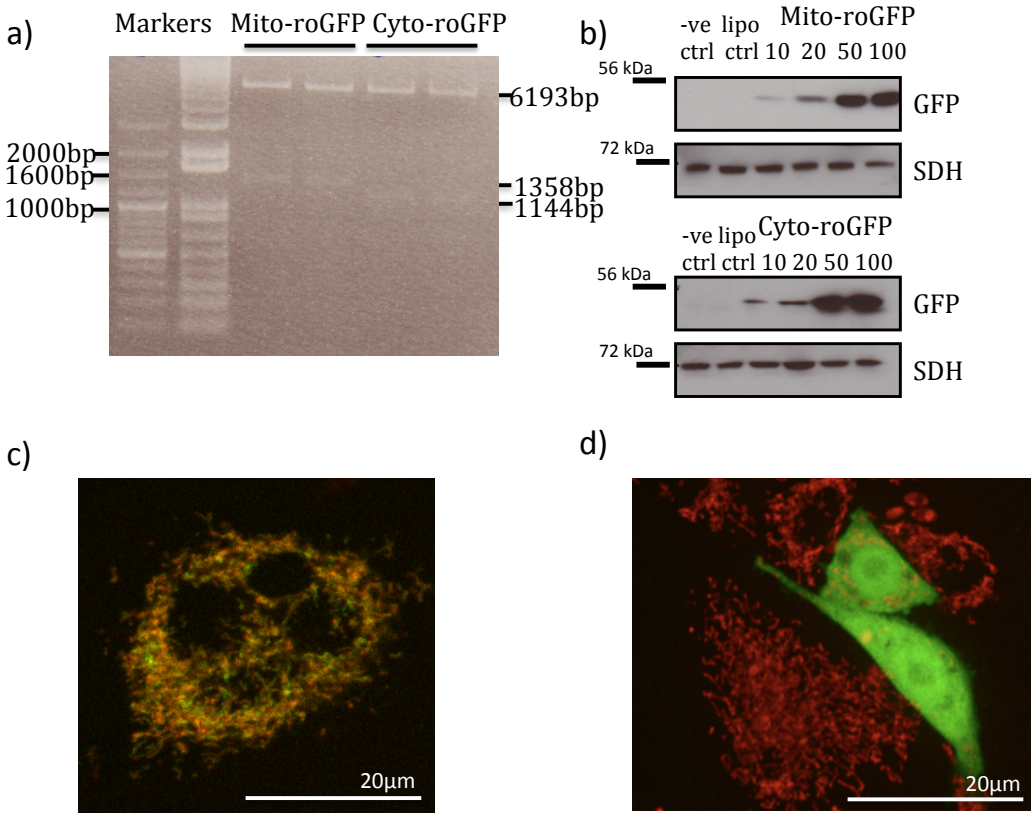
a)
Markers
Mito-roGFP
Cyto-roGFP
2000bp
1600bp
1000bp
6193bp
1358bp
1144bp
b)
-ve ctrl
lipo ctrl
Mito-roGFP
10 20 50 100
56 kDa
GFP
72 kDa
SDH
-ve ctrl
lipo ctrl
Cyto-roGFP
10 20 50 100
56 kDa
GFP
72 kDa
SDH
c)
20µm
d)
20µm

Figure 4- CHO cells show a high transfection efficiency and show proper localization of cytosolic and mitochondrial targeted redox sensitive GFP. a) Plasmid DNA encoding mito-Grx1-roGFP and cyto-Grx1-roGFP were transformed into DH5α *E. coli* and grown up for purification. Resultant DNA samples were subjected to restriction enzyme digestion with *Cla*I and *Bgl*II enzymes and run on a 0.8% agarose gel to confirm their identity. b) Subsequently DNA preparations were transfected with increasing amounts of DNA (10µg/mL-100µg/mL) into CHO cells, and then cells were lysed for protein collection. 30µg of protein was then run on a reducing SDS-PAGE gel and Western blotted for GFP expression; -ve ctrl: Untransfected CHOEV cells, lipo ctrl; transfection conditions no DNA added. Succinate dehydrogenase was used to assess equal loading of samples. c) and d) show the visualization of mito-Grx1-roGFP and cyto-Grx1-roGFP (green) in transfected CHO cells, respectively, stained with TMRE (red).

cells expressing UCP3 (Figure 5a). This finding was supported by the observation that the medium in which the cells were cultured became acidic quickly. Perhaps this cell line experienced high PMF, low ATP demands and consequently high ROS emissions. Perhaps the ectopic expression of UCP3 in this cell line may enable these cells to modulate PMF sufficiently in order to avoid shunting towards glycolysis dependent ATP production. Following measurement of the resting oxygen consumption rate (OCR), oligomycin-induced state 4 (state 4_o) was measured. Results showed that there was no effect of oligomycin in CHOEV cells. This, along with the abnormally low resting respiration rates, suggests that these cells have very low mitochondrial oxygen consumption rates and reduced capacity for mitochondrial oxidative phosphorylation function (Figure 5b). Additionally, some of the observed respiration rates were negative. Upon visual assessment it was clear that their ability to adhere to the culture dish, even with Matrigel coating, was poor. As such, mixing phases during the experiment resulted in lifting of cells and which may have coincided with probe measurement areas. As a result of these findings, a new model system was required to achieve my research objectives. The Human Embryonic Kidney (HEK293) cell line was then chosen as a model system. HEK293 cells are easy to transfect and this was considered as an advantage for our planned biosensor experiments. In addition, we acquired the mitochondrial targeted hydrogen peroxide specific YFP biosensor, pHyPer-dmito, to include in our analyses.

Optimization of transfection conditions for the three fluorescent probes in HEK293 cells showed that HEK293 cells have high transfection and expression efficiency. No difference was observed with the use of increasing amounts of DNA (Figures 6a). Both the

Figure 5

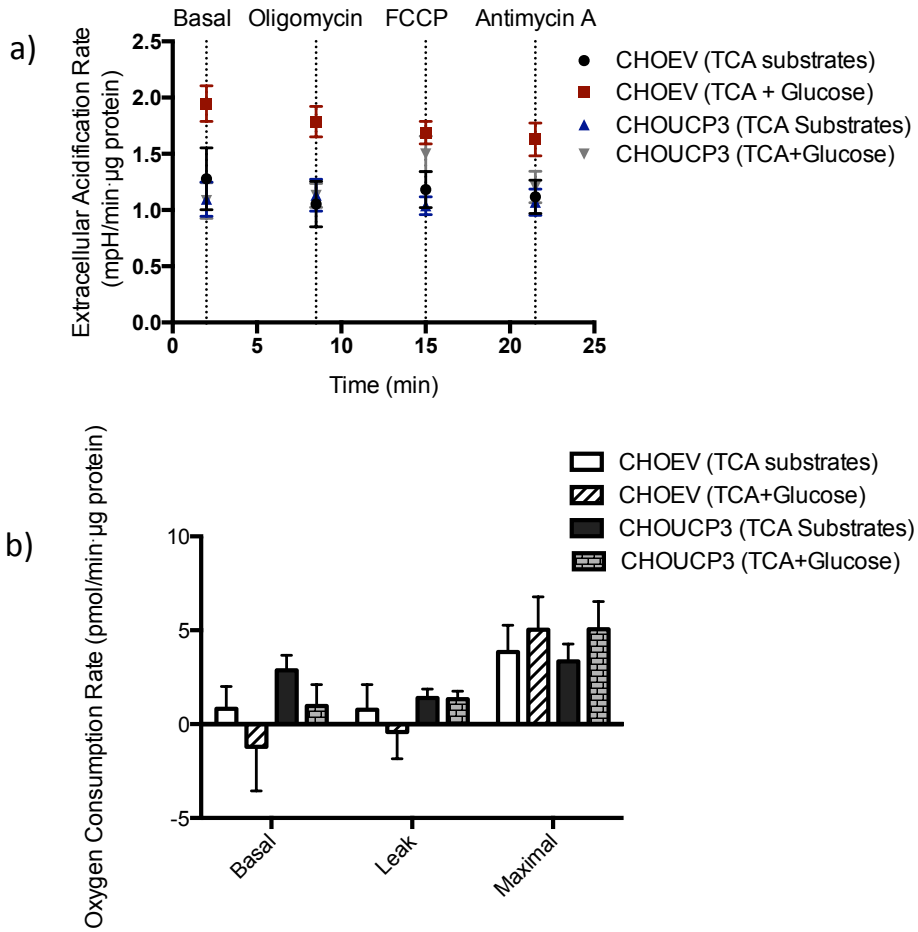
a)
Basal
Oligomycin
FCCP
Antimycin A
Extracellular Acidification Rate (mpH/min·µg protein)
2.5
2.0
1.5
1.0
0.5
0.0
0
5
10
15
20
25
Time (min)
CHOEV (TCA substrates)
CHOEV (TCA + Glucose)
CHOUCP3 (TCA Substrates)
CHOUCP3 (TCA+Glucose)
b)
Oxygen Consumption Rate (pmol/min·µg protein)
10
5
0
-5
Basal
Leak
Maximal
CHOEV (TCA substrates)
CHOEV (TCA+Glucose)
CHOUCP3 (TCA Substrates)
CHOUCP3 (TCA+Glucose)

Figure 5- CHO cells exhibit poor capacity for mitochondrial oxidative phosphorylation. CHO cells containing stably expressing empty vector (EV) or uncoupling protein 3 (UCP3). Cultured cells were placed in media containing TCA cycle substrates (4mM L-glutamine, 1mM sodium pyruvate) ±25mM glucose. a) Extracellular acidification rate (ECAR) as a proxy measure of glycolytic flux. b) Oxygen consumption rate as a measure of electron transport chain (ETC) flux. (Average±SEM, n=6)

Figure 6

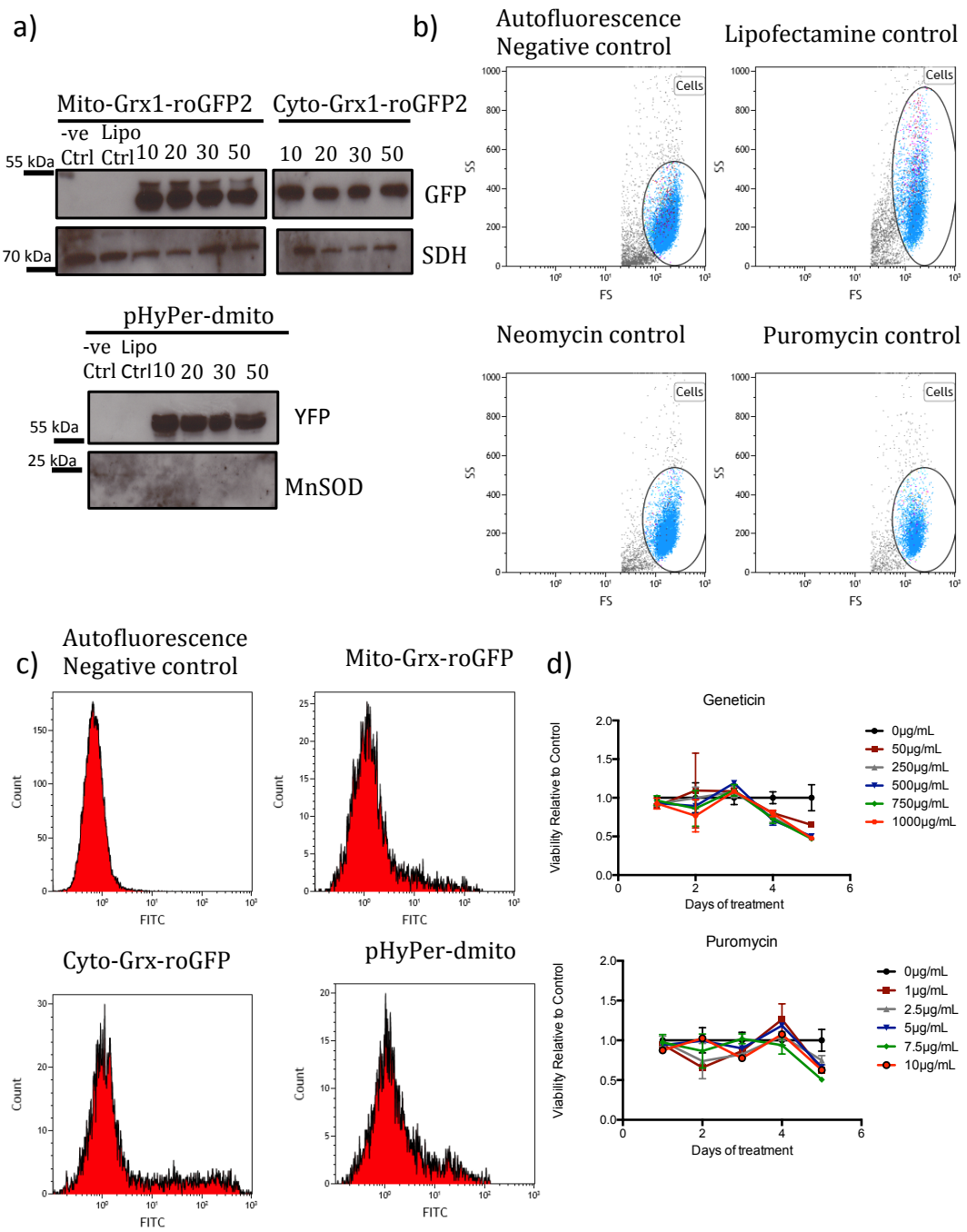
a)
Mito-Grx1-roGFP2
Cyto-Grx1-roGFP2
-ve Ctrl
Lipo Ctrl
10 20 30 50
10 20 30 50
55 kDa
GFP
70 kDa
SDH
pHyPer-dmito
-ve Ctrl
Lipo Ctrl
10 20 30 50
55 kDa
YFP
25 kDa
MnSOD
b)
Autofluorescence Negative control
Lipofectamine control
Neomycin control
Puromycin control
Cells
SS
FS
c)
Autofluorescence Negative control
Mito-Grx-roGFP
Cyto-Grx-roGFP
pHyPer-dmito
Count
FITC
d)
Geneticin
Viability Relative to Control
Days of treatment
0µg/mL
50µg/mL
250µg/mL
500µg/mL
750µg/mL
1000µg/mL
Puromycin
0µg/mL
1µg/mL
2.5µg/mL
5µg/mL
7.5µg/mL
10µg/mL

Figure 6- Effective lipofectamine transfection of fluorescent biosensors and the increased granularity of cells. The effect of the transfection process and antibiotic selection on the cell population. a) DNA preparations were transfected with increasing amounts of DNA (10µg/mL-100µg/mL) into HEK293 cells and cells were lysed for protein collection and 30µg of protein was run on a reducing SDS-PAGE gel and Western blotted for GFP or YFP expression; -ve ctrl: Untransfected CHOEV cells, lipo ctrl; transfection conditions no DNA added. Succinate dehydrogenase or manganese superoxide dismutase were used to asses equal loading of samples b) Flow cytometry assessment of the effects of lipofectamine and antibiotic treatments on cells physical characteristics. c) Flow cytometry assessment of the expression of fluorescent biosensors transiently transfected into HEK293 cells. d) Kill curves showing viability of HEK293 cells determined by an MTT assay over 6 days of treatment with various concentration of geneticin and puromycin (Average±SEM, n=3)

effect of the transfection treatment as well as the presence of the fluorescent probe protein were further assessed using flow cytometry. The Lipofectamine treatment increased cellular complexity/granularity with little effect on the fluorescent background in the cells (Figure 6b). Flow cytometry showed a transfection efficiency of 15%, 6% and 18% for mito-Grx1-roGFP, Cyto-Grx1-roGFP and pHyPer-dmito, respectively (Figure 6c).

In order to create a more flexible model system in which mSOF could be studied, a decision was made to create stable transfects that express each of the probes. Analyses could thus be carried out in a much more timely and cost effective manner; stable cells were thought to also offer greater flexibility for future directions of the project. In order to create stably expressing cells for each of the three probes, kill curves were conducted and appropriate concentrations of antibiotics (either puromycin or geneticin) were determined for proper selection (Figure 6b). From the kill curve results, a concentration of 750µg/mL geneticin was chosen to select HEK293-pHyPer-dmito stables, while 7.5µg/mL puromycin was chosen for HEK293-Mito-Grx1-roGFP2 and HEK293-Cyto-Grx1-roGFP2. In addition, flow cytometry was employed to assess the effect of drug selection with a 24h treatment; there were no noticeable effects on fluorescence, compared to control cells (Figure 6d). While HEK293-pHyPer-dmito stables performed well during selection, both the Mito-Grx1-roGFP2 and Cyto-Grx1-roGFP2 were eradicated. This may have been due to excessive concentrations of puromycin during selection, or to reduced expression of the resistance gene by the cells. Upon reconsideration of the kill curve experiments it was noted that 100% eradication was not reached during the 6 d time course.

The successful HEK293-pHyPer-dmito stable transfects were assessed for their expression of the pHyper-dmito probe in three ways. First cells were imaged with both transmitted and fluorescent light, and it was found that close to 40% of cells expressed the probe (Figure 7a). To strengthen these data a Western blot confirmed the presence of pHyPer-dmito in stable transfect cell lysates (Figure 7b). Lastly, HEK293-pHyPer-dmito stable transfects were analyzed using flow cytometry, and it was found that some cells had lost their fluorescence and 25% of cells analyzed expressed the probe of interest (Figure 7c). Since kill curves were insufficient at providing the proper concentration at which cells should be selected clonal cell line production was not achieved. In order to develop a non-clonal cell line with the transfected cell the population was subsequently sorted using fluorescent activated cell sorting (FACS) in order to create four non-clonal, 100% expressing populations (Figure 7c). These four populations again were subjected to Western blotting to confirm their expression of YFP (Figure 7d). A decision was made to continue with the HEK293-pHyPer-dmito expressing cells for further determinations of flash events following the dismutation of superoxide to H_2O_2. The underlying rationale behind the use of this biosensor was the importance of H_2O_2 as a membrane traversing signaling molecule that governs many cellular processes. In other words, if these mSOF are of physiological significance in this respect it is imperative that we are able to observe them in an applicable manner (*e.g.* as ROS flash events).

4.2 Kinetic assessment of hydrogen peroxide specific biosensor

The YFP brightness of these four expressing populations was noted to be moderate as observed on the wide-field deconvolution-based DeltaVision CORE microscope allowing for the monitoring of both increases and decreases in H_2O_2-associated fluorescence in the

Figure 7

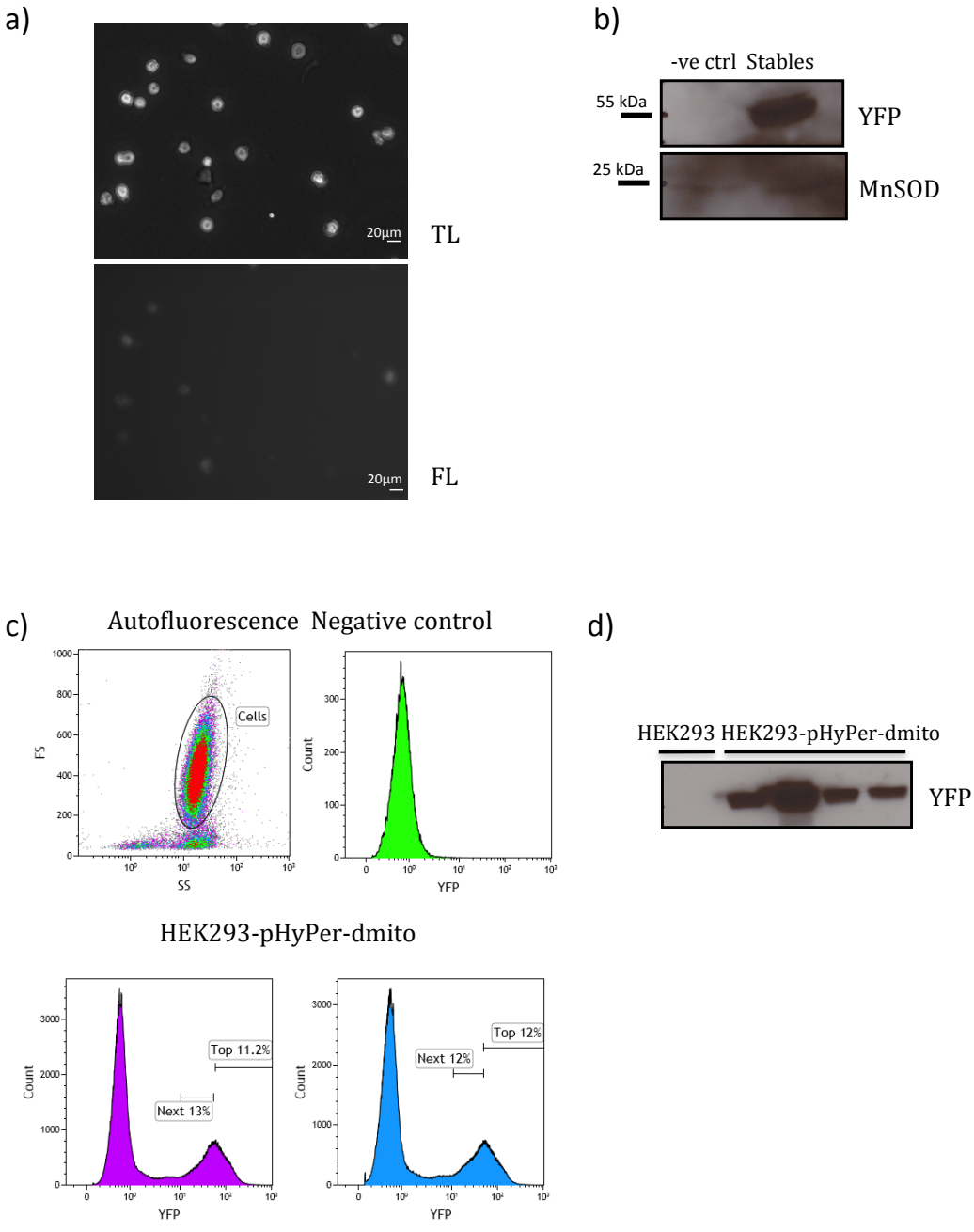
a)
20µm
TL
20µm
FL
b)
-ve ctrl
Stables
55 kDa
YFP
25 kDa
MnSOD
c)
Autofluorescence
Negative control
Cells
FS
SS
Count
YFP
HEK293-pHyPer-dmito
Top 11.2%
Next 13%
Top 12%
Next 12%
d)
HEK293
HEK293-pHyPer-dmito
YFP

Figure 7- A subpopulation of pHyper-dmito transfected cells express YFP. a) HEK293 cells were transiently transfected with p-HyPer-dmito and selected for with 750µg/mL geneticin for 10 days and cells were imaged. ~40% of cells were found to express this YFP biosensor (FL) observed under transmitted light (TL). b) Western blot for YFP expression in untransfected (-ve ctrl) and HEK293 cells transfected with p-HyPer-dmito and selected for with 750µg/mL geneticin for 10days. Manganese superoxide dismutase (MnSOD) was used to asses equal loading of samples. c) Two non-clonal pHyPer-dmito expressing HEK293 cell populations were sorted using FACS to get four 100% expressing cell lines. d) Untransfected HEK293 and the sorted cell lines were Western blotted for YFP expression.

Figure 8

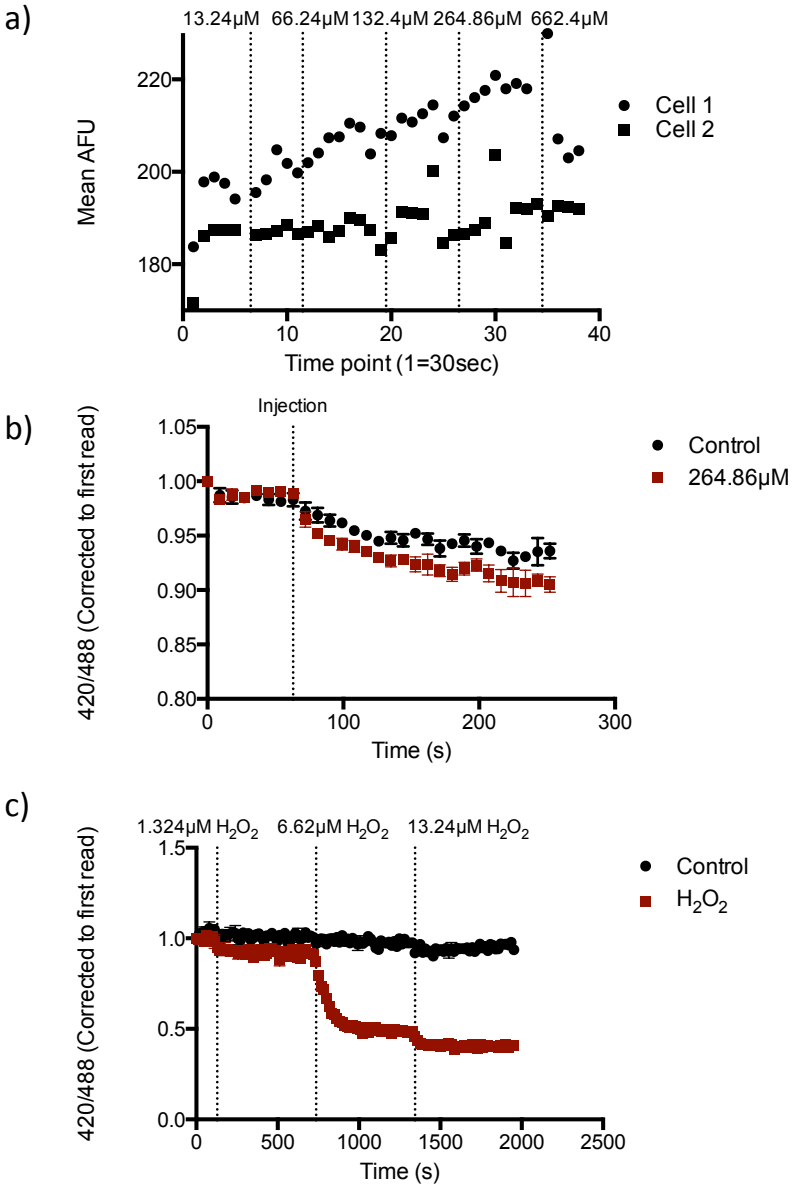
a)
13.24μM
66.24μM
132.4μM
264.86μM
662.4μM
Mean AFU
220
200
180
0
10
20
30
40
Time point (1=30sec)
Cell 1
Cell 2
b)
Injection
420/488 (Corrected to first read)
1.05
1.00
0.95
0.90
0.85
0.80
0
100
200
300
Time (s)
Control
264.86μM
c)
1.324μM H2O2
6.62μM H2O2
13.24μM H2O2
420/488 (Corrected to first read)
1.5
1.0
0.5
0.0
0
500
1000
1500
2000
2500
Time (s)
Control
H2O2

Figure 8- The oxidation of pHyPer-dmito is detectable in a ratiometric manner. a) Proof of concept experiment demonstrating the increase in ex488/em516 fluorescence in response to exogenous titration of H_2O_2 (two individual cells) Ratiometric response (420/488) of pHyPer-dmito corrected to first read values of HEK293-pHyPer-dmito fluorescence measured at ex420/em516 and ex488/em516 b) Intact cells treated with exogenous H_2O_2 using microplate reader assay with poor SNR. c) 45µg cell free extract protein in response to exogenous H_2O_2 titration over time. (Average±SEM, n=3)

mitochondria. Functionality of the probe in the stable cell population was briefly tested by the sequential addition of exogenous H_2O_2 to cells while monitoring ex488nm/em535nm (Figure 8a). pHyPer-dmito, previously characterized as a H_2O_2 sensitive probe lacks information on kinetics of its reaction. Since this probe was to be implemented in order to monitor dynamic changes in H_2O_2 on a short time scale, it was important to know its kinetic parameters. Due to accessibility, a microplate reader assay was developed to assess the sensitivity and kinetics of pHyPer-dmito on a cell population level. Initially changes in 420nm/488nm, corrected to the initial reads, were assessed for the exogenous addition of H_2O_2 to intact cells. The recorded changes were small compared to controls even at H_2O_2 concentrations significantly greater than physiological levels yielding low signal to noise ratio difficult for kinetic determinations (Figure 8b).

To improve the sensitivity of this assay we chose to develop an isolation procedure for a cell free system enabling greater amounts of probe to be available in each well during the assay as well as more direct access to the probe. The resultant homogenate, cell free extract, was found to produce a more sensitive, reproducible response. Initially, responsiveness to physiological concentrations of H_2O_2 was carried out showing sequential exogenous addition of H_2O_2 (Figure 8c). Additionally, endogenous recovery of the signal to a baseline level was assessed by monitoring changes in 420nm/488nm over time following H_2O_2 addition (Figure 9a). This yielded recovery times similar to those reported by Malinouski *et al*. ~40min. Malinouski *et al*. began characterization of this probe by carrying out proof-of-concept experiments showing the reversibility of the probe to the reduced state using DTT (Malinouski et al., 2011). When these experiments were carried out in our laboratory however, it was clear that there is no difference in the kinetics of recovery in the

Figure 9

a)

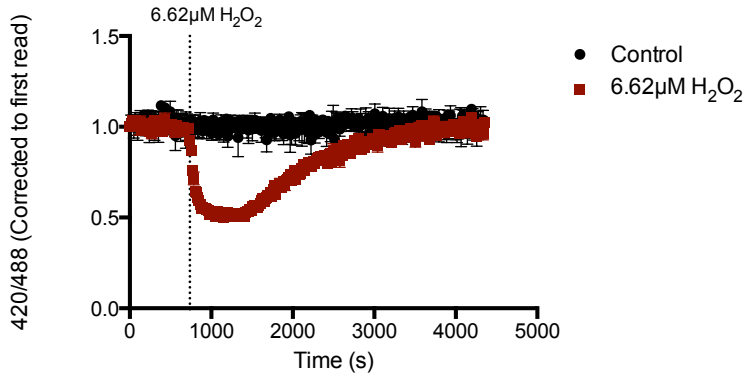
6.62μM H_2O_2
420/488 (Corrected to first read)
1.5
1.0
0.5
0.0
0
1000
2000
3000
4000
5000
Time (s)
Control
6.62μM H_2O_2

b)

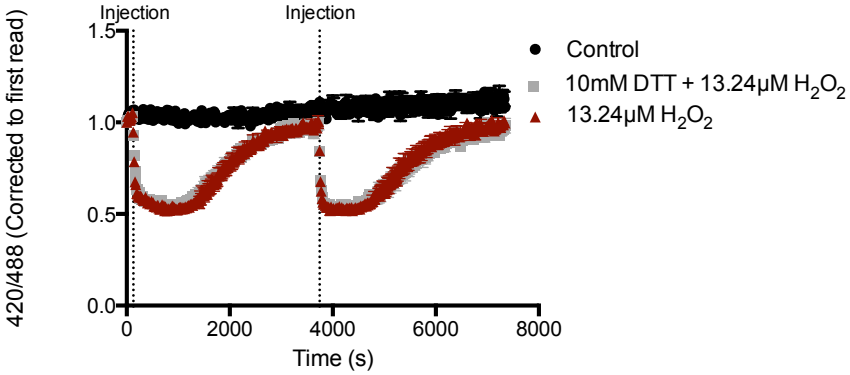
Injection
Injection
420/488 (Corrected to first read)
1.5
1.0
0.5
0.0
0
2000
4000
6000
8000
Time (s)
Control
10mM DTT + 13.24μM H_2O_2
13.24μM H_2O_2

Figure 9- The reversible oxidation of pHyPer-dmito is mediated by endogenous reductants. Ratiometric response (420/488) and recovery of 45µg protein fromHEK293-pHyPer-dmito cell free extract corrected to first read values of HEK293-pHyPer-dmito fluorescence measured at ex420/em516 and ex488/em516 a) Oxidation and recovery in response to the addition of 6.62µM H_2O_2 monitored over time and B) Response to the exogenous addition of 13.24µM H_2O_2 ±10mM DTT addition and subsequent oxidation and reversibility after the second addition of H_2O_2. (Average ± SEM, n=3-4).

r presence or absence of excess DTT (Figure 9b). These data suggest reversibility of HyPer is modulated by endogenous reductive enzyme couples (*e.g.,* thioredoxin/thioredoxin eductase/NADPH, glutaredoxin/glutathione/glutathione reductase/NADPH, or lipoic acid/thioredoxin reductase/NADPH) and is unaltered by exogenous changes in redox state.

Using this model we were able to assess the kinetics *in vitro* of pHyPer-dmito. Exogenous addition of varying concentrations of H_2O_2 allowed for the calculation of Michaelis-Menton kinetics. The creation of a Lineweaver-Burk plot allowed for the determinations of the K_m (7.18μM) and V_{max} (-0.012$\Delta\frac{420}{488}s^{-1}$) for the reaction between pHyPer –dmito and exogenous H_2O_2 *in vitro* (Figure 10). The kinetics of pHyPer-dmito were found to be too slow to monitor dynamic fluctuations of H_2O_2 concentrations in the context of ROS flashes, which occur on a timescale of ~20s.

4.3 Contribution of UCP3 in the regulation of mSOF events

Following kinetic characterization of the pHyPer-dmito probe it was obvious that while it was sensitive enough to detect fluctuations in H_2O_2 production at physiological levels it lacked the requisite kinetics that would enable detection of changes in ROS production observed during mSOF. For this reason we again switched our focus and began to use the established mitochondrial targeted, superoxide specific YFP biosensor, mt-cpYFP to assess the contribution of UCP3 in the regulation of mSOF events.

In order to assess the contribution of UCP3 in the regulation of mSOF events WT and UCP3KO mice were sent to the laboratory of Dr. Robert Dirksen at the University of

Figure 10

a)

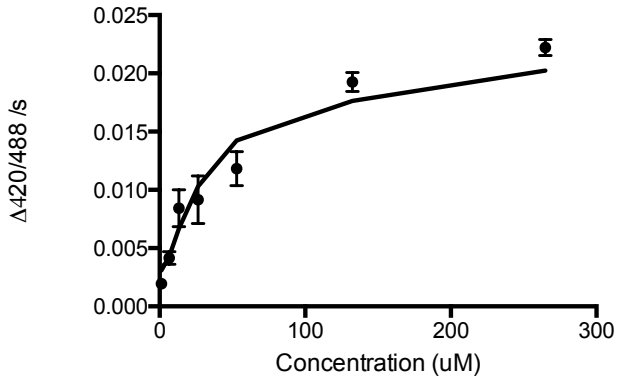
0.025
0.020
0.015
0.010
0.005
0.000
Δ420/488 /s
0
100
200
300
Concentration (uM)

b)

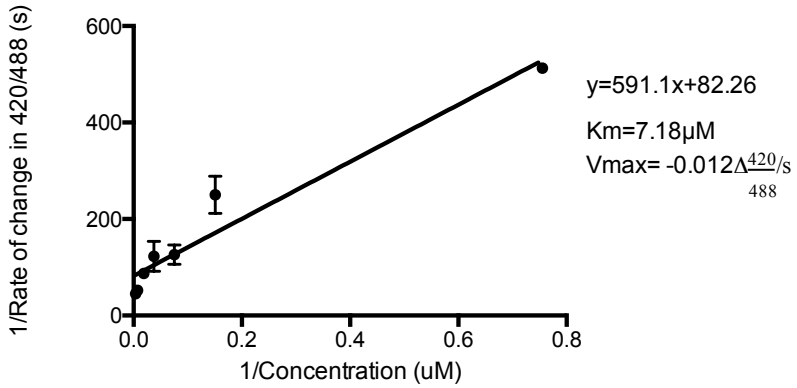
600
400
200
0
1/Rate of change in 420/488 (s)
0.0
0.2
0.4
0.6
0.8
1/Concentration (uM)
y=591.1x+82.26
Km=7.18μM
Vmax= -0.012Δ420/s
488

Figure 10- Characterization of pHyPer-dmito Michaelis-Menten kinetics in a cell free system. Plotted rate of change in 420/488 ratio of pHyPer-dmito probe monitored in response to the addition of various concentrations of exogenously added hydrogen peroxide. a) Michaelis-Menten model of calculated rates following the exogenous addition of H_2O_2 B) Lineweaver-Burk plot of kinetics data for determination of Km (7.18µM) and Vmax (-0.012Δ420/488s^{-1}). (Average ± SEM, n=3)

Rochester Medical Center. In a collaborative effort, mice were electroporated with mt-cpYFP a mitochondrial targeted, superoxide specific YFP for detection of changes in superoxide production. mSOF determinations were carried out on FDB muscle fibers. The resultant image series were used in the analysis flash characteristics in both WT and UCP3KO mice using a developed MATLAB based command line prompt, 'Flash Collector'. This software detects mSOF events and characterizes them computing information about flash frequency, amplitude, full duration at half maximum (FDHM), decay constant, time-to-peak, duration and flash area (Figure 11). While many characteristics were unchanged, analyses showed that the average area of the flashes in UCP3KO mice was smaller than that observed in WT mice ($n=4$, $p<0.01$) (Figure 11c). Additionally, a prolonged duration of flashes in the UCP3KO muscle, compared to WT muscle ($n=4$, $p=0.04$) was observed (Figure 11d).

Since an increased flash duration in UCP3KO was observed, it was of interest to see whether there was a difference in spread for FDHM across all individually measured flashes as an indication of the duration of the flash peak. There was however no difference in the spread of FDHM graphed for individual flashes between WT and UCP3 KO mice ($n=459$-504, $p=0.91$).

Furthermore, a similar analysis was carried out to assess whether the observed smaller flash area was due to an inherent incapability for larger flash area due to mitochondrial size and ultrastructure. First, the areas of all flashes were graphed noting that the largest flash in each genotype was of a similar area. From this it was noted that both

Figure 11

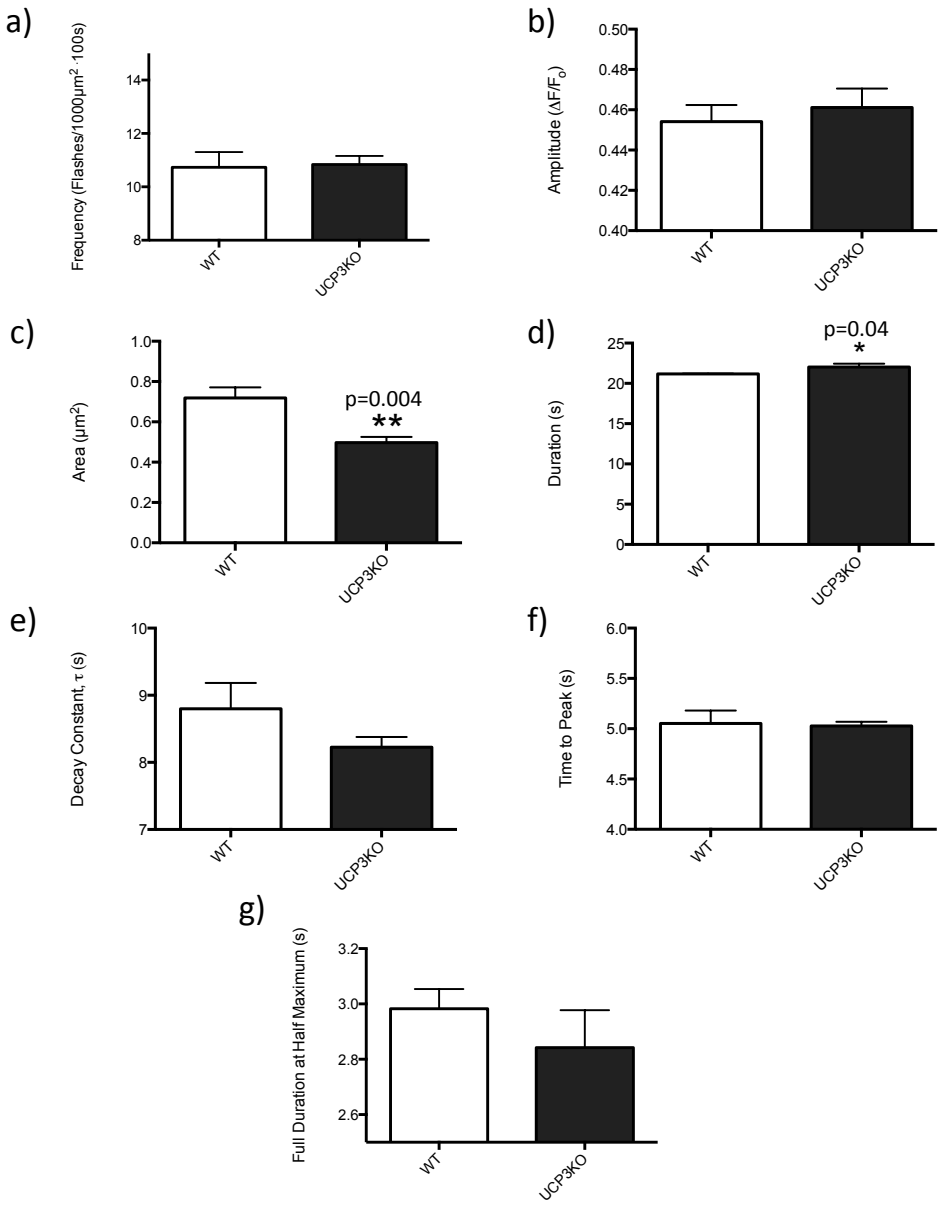
a)
Frequency (Flashes/1000μm² ·100s)
14
12
10
8
WT
UCP3KO
b)
Amplitude (ΔF/F₀)
0.50
0.48
0.46
0.44
0.42
0.40
WT
UCP3KO
c)
Area (μm²)
1.0
0.8
0.6
0.4
0.2
0.0
p=0.004
**
WT
UCP3KO
d)
Duration (s)
25
20
15
10
5
0
p=0.04
*
WT
UCP3KO
e)
Decay Constant, τ (s)
10
9
8
7
WT
UCP3KO
f)
Time to Peak (s)
6.0
5.5
5.0
4.5
4.0
WT
UCP3KO
g)
Full Duration at Half Maximum (s)
3.2
3.0
2.8
2.6
WT
UCP3KO

Figure 11- UCP3KO mouse FDB exhibit mSOF events having a greater duration and a smaller area (μm^2) compared to FDB of WT mice. mSOF characteristics calculated by 'Flash Collector' executed in MATLAB from time series acquired monitoring mt-cpYFP fluorescence in isolated myofibers from flexor digitorum brevis of WT and UCP3KO mice. a) Flash frequency b) Flash amplitude c) Flash area d) Flash duration e) Decay constant of flash f) Time to flash peak g) Full Duration at Half Maximum. Student's *t*-test (Average±SEM, n=4)

genotypes were capable of producing large flashes. When the spread of these data were compared, we noted a statistically significant difference in the skew of the data, thereby demonstrating a greater number of large flash events in WT than UCP3KO muscle ($p<0.0001$).

Since these events have been defined as non-propagating and have been noted to occur in single or connected mitochondria an assessment of the size of mitochondria in muscle from both groups of mice was carried out using high resolution electron microscopy (EM). Results revealed that mitochondria in UCP3KO FDB were in fact smaller than their WT counterparts, implicating the smaller area for observed mSOF known to occur in single or connected mitochondria ($p=0.032$) (Figure 12).

4.4 Defining the relationship between mSOF and mitochondrial depolarizations

Analyses were sought to examine whether there was a difference in the depolarization amplitude (*i.e.*, dips in TMRE fluorescence) concomitant with mSOF events. As described above, previous research has established that UCP3 is a transmembrane protein involved in regulating membrane potential in highly polarized states such as those observed in times of high ROS production. Although the difference between WT and UCP3KO was not significant ($p=0.38$), we did however find and quantify a novel linear correlation between flash intensity and depolarization intensity ($R^2_{WT}=0.63477$ and $R^2_{KO}=0.72044$) (Figure 13). In order to further understand mSOF regulation we set out to temporally resolve the occurrence of the mSOF with the observed mitochondrial depolarization. Using mt-cpYFP transgenic mice isolated muscle fibers stained with TMRE images acquired at top speed

Figure 12

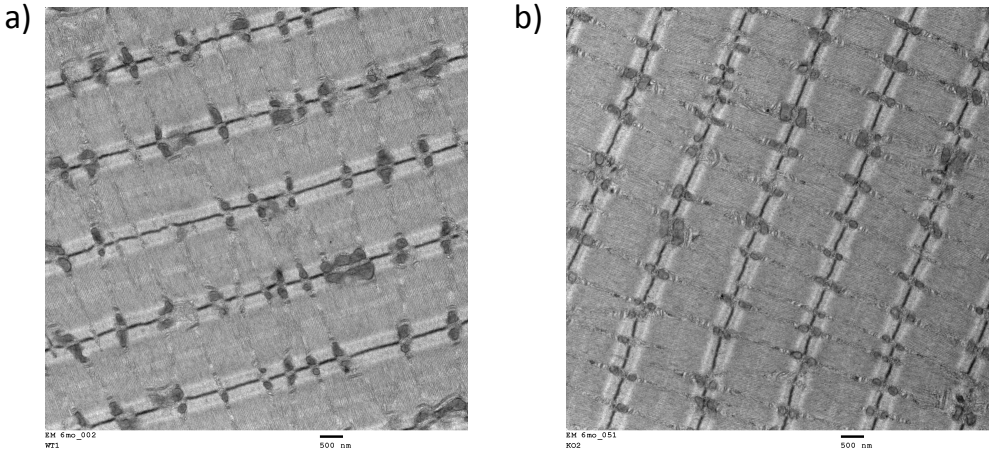
a)
EM 6mo_002
WT1
500 nm
b)
EM 6mo_051
KO2
500 nm

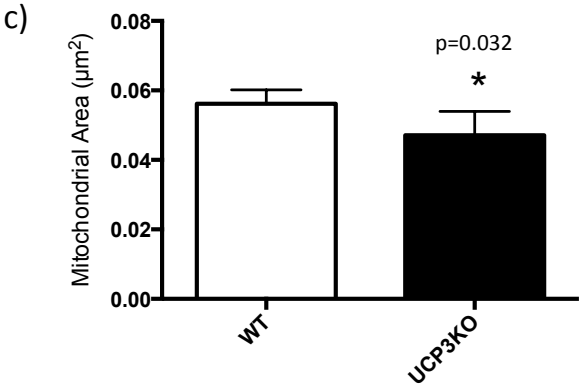
c)
Mitochondrial Area (µm2)
0.08
0.06
0.04
0.02
0.00
p=0.032
*
WT
UCP3KO

Figure 12- Muscle fiber mitochondria of UCP3KO mice are smaller than their WT counterparts. a) & b) Representative EM images of flexor digitorum brevis muscle of WT and UCP3KO respectively used for analysis of mitochondrial area c) Average area of measured mitochondria. Mitochondrial area in UCP3KO muscle was smaller than that in muscle of WT mice.(Average±SEM) (n=4, p=0.032).

Figure 13

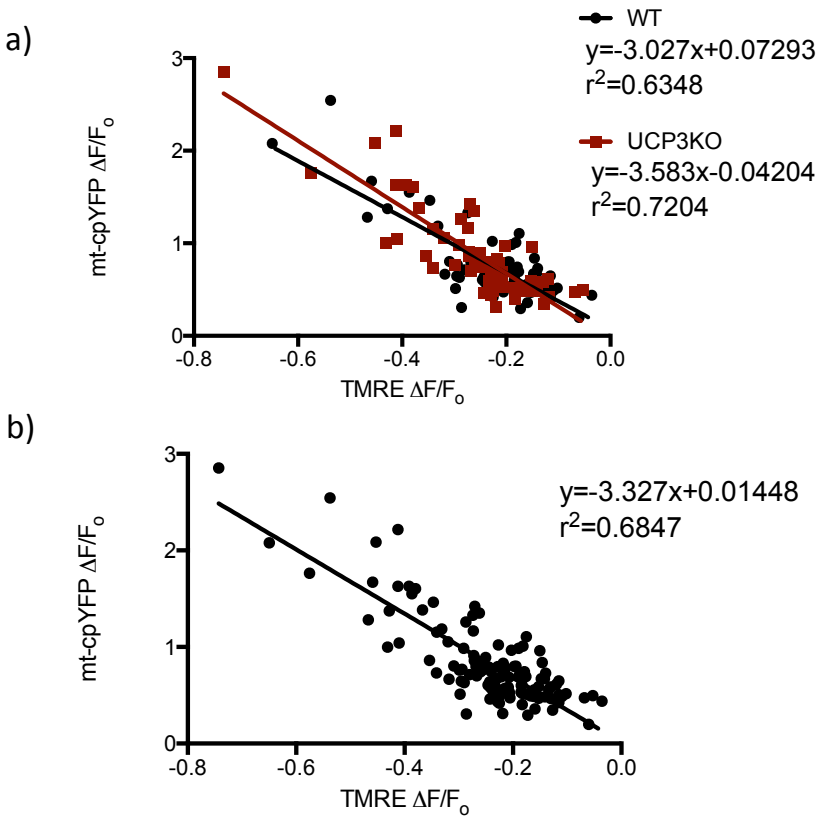
a)
WT
y=-3.027x+0.07293
r2=0.6348
UCP3KO
y=-3.583x-0.04204
r2=0.7204
mt-cpYFP ΔF/Fo
TMRE ΔF/Fo
b)
y=-3.327x+0.01448
r2=0.6847
mt-cpYFP ΔF/Fo
TMRE ΔF/Fo

Figure 13- Genotype independent correlation between flash intensity and the magnitude of MIM depolarization. Single flash analyses of the amplitude of mt-cpYFP flashes and concomitant mitochondrial depolarization events (TMRE fluorescence). a) Comparison of the correlation of these two events in WT and UCP3KO muscle. ANOVA F-test (n=59-62, p=0.38) and b) Combined, genotype independent, data defining the novel correlation revealed (n=112, r=0.6874, p<0.0001)

using spinning disk confocal technology proved too slow to discern the resolution of events (data not shown).

4.5 Comparison of mSOF characteristics among skeletal muscles of various fiber type compositions

Following collection of images under conditions very similar to those used in Rochester we established an optimized set of analysis parameters in which we were able to pick up the majority of observed flashes without picking up background fluctuations as part of the analysis. Average values obtained from a series of experiments were graphically and statistically compared to the values previously seen in WT mouse FDB (Figure 14). There was no difference in almost all parameters measured however; curiously there was great statistical significance in the measured full duration at half maximum suggesting a prolonged peak of the measured flashes ($P<0.0001$).

Following this establishment of methods, analyses were carried out to examine whether these metabolically linked events differed based on fiber type composition. In order to do this, measurements of mSOF were carried out in soleus (more oxidative type fibers) and EDL (more glycolytic type fibers). Unfortunately, in these preliminary experiments no statistically significant differences were detected in mSOF frequency or other characteristics in these muscles having greatly divergent fiber type compositions (Figure 15). Finally, primary myoblasts from these mice were isolated from mt-cpYFP for future projects in the laboratory.

Figure 14

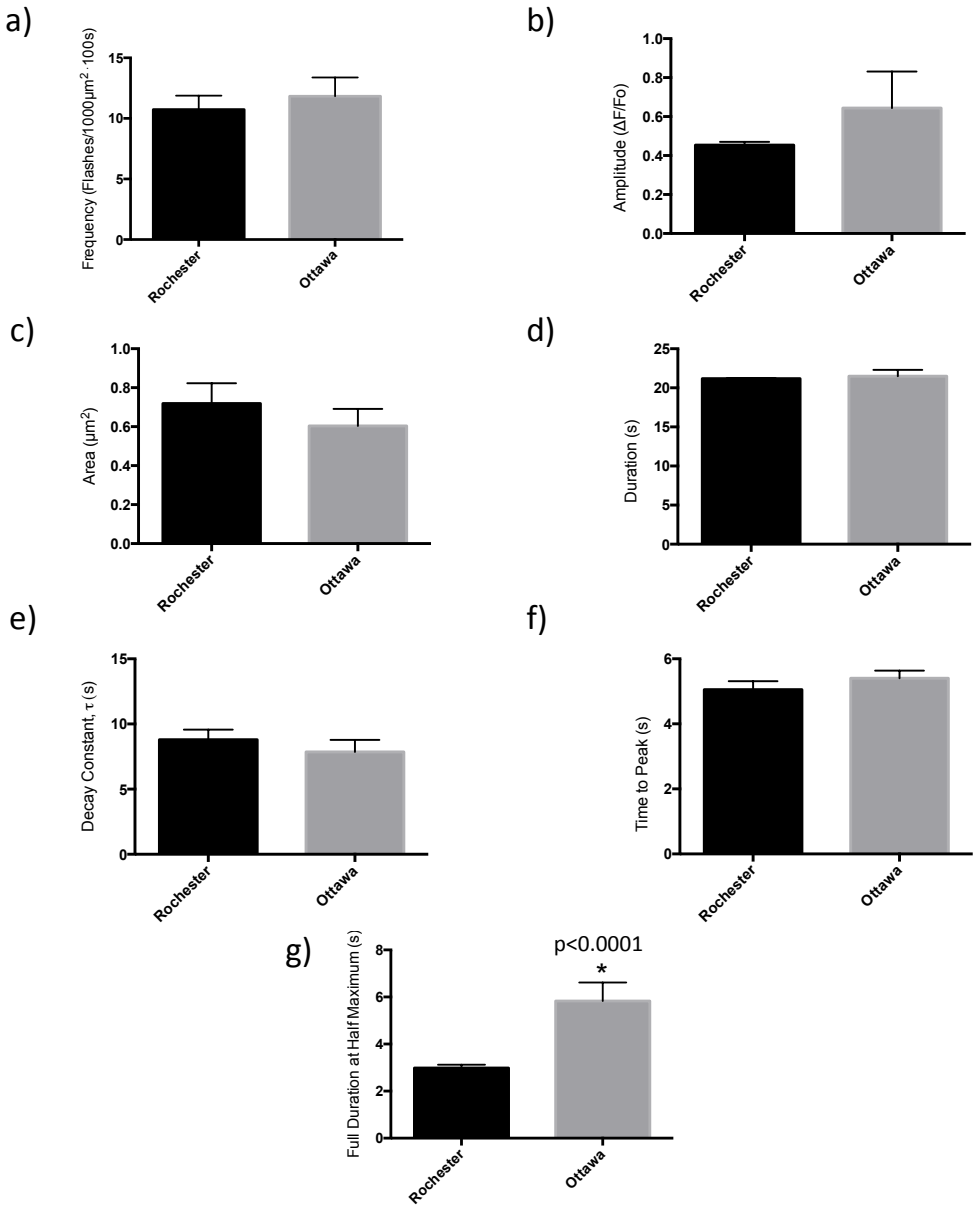
a)
Frequency (Flashes/1000μm²·100s)
15
10
5
0
Rochester
Ottawa
b)
Amplitude (ΔF/Fo)
1.0
0.8
0.6
0.4
0.2
0.0
Rochester
Ottawa
c)
Area (μm²)
1.0
0.8
0.6
0.4
0.2
0.0
Rochester
Ottawa
d)
Duration (s)
25
20
15
10
5
0
Rochester
Ottawa
e)
Decay Constant, τ (s)
15
10
5
0
Rochester
Ottawa
f)
Time to Peak (s)
6
4
2
0
Rochester
Ottawa
g)
Full Duration at Half Maximum (s)
p<0.0001
*
8
6
4
2
0
Rochester
Ottawa

Figure 14- Optimized measurements FDB of WT mice on spinning disk confocal microscope in Ottawa exhibit similar characteristics as those measured in Rochester. MATLAB analysis of mSOF event characteristics imaged from flexor digitorum brevis of WT mice both in Rochester and in Ottawa. a) Flash frequency b) Flash amplitude c) Flash area d) Flash duration e) Decay constant of flash f) Time to flash peak g) Full Duration at Half Maximum. Student's *t*-test (Average±SEM, n=4-6)

Figure 15

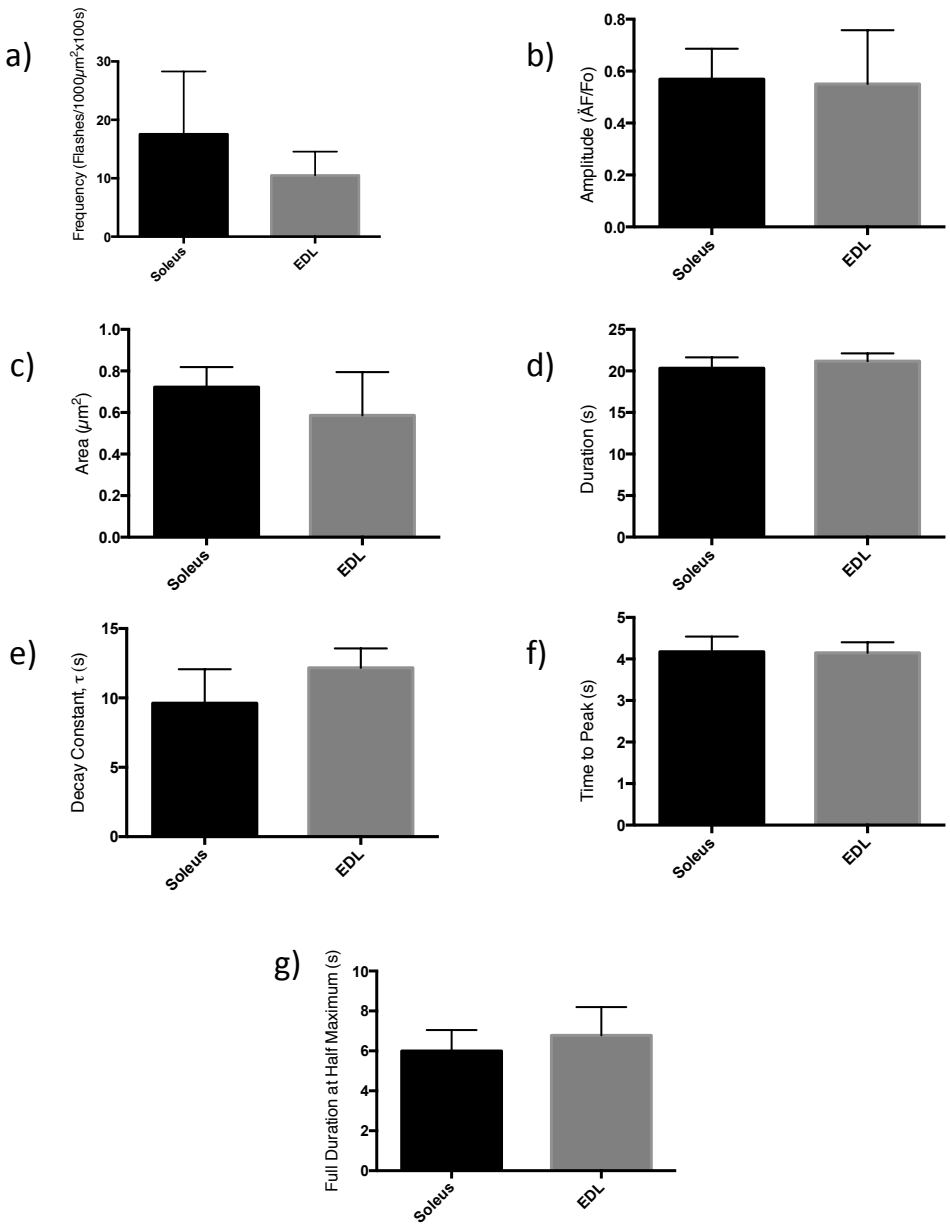
a)
Frequency (Flashes/1000μm²x100s)
30
20
10
0
Soleus
EDL
b)
Amplitude (ΔF/Fo)
0.8
0.6
0.4
0.2
0.0
Soleus
EDL
c)
Area (μm²)
1.0
0.8
0.6
0.4
0.2
0.0
Soleus
EDL
d)
Duration (s)
25
20
15
10
5
0
Soleus
EDL
e)
Decay Constant, τ (s)
15
10
5
0
Soleus
EDL
f)
Time to Peak (s)
5
4
3
2
1
0
Soleus
EDL
g)
Full Duration at Half Maximum (s)
10
8
6
4
2
0
Soleus
EDL

Figure 15- No difference in flash characteristics between muscles having greatly different proportions of oxidative and glycolytic fibers. MATLAB analysis of mSOF event characteristics imaged from flexor digitorum brevis (FDB), soleus and extensor digitorum longus (EDL) of mt-cpYFP transgenic mice. a) Flash frequency b) Flash amplitude c) Flash area d) Flash duration e) Decay constant of flash f) Time to flash peak g) Full Duration at Half Maximum. Student's *t*-test (Average±SEM, n=4)

5.0 DISCUSSION:

Cellular ROS levels exist as a dynamic equilibrium between ROS production and detoxification. Originally, ROS were considered to be solely toxic due to their reactive nature with DNA, lipids, proteins and other biomolecules, causing oxidative damage (Murphy, 2009). More recently the identification of ROS as important signaling molecules has opened new doors in ROS and mitochondrial research. Moreover, impaired ROS handling has increasingly been associated with a very wide range of disease states. However, mechanistic details are lacking and thus an improved understanding of ROS biology is relevant to potential preventative and therapeutic strategies for many diseases.

The **overall aim of my project** was to establish methods to investigate the characteristics and mechanistic details governing mSOF in skeletal muscle. It was hypothesized that UCP3 plays a role in governing mSOF events. This governance occurs through modulation of mitochondrial membrane potential through leak mechanisms, which are temporally linked to the observed mSOF.

Within the last five years mitochondrial and ROS research has uncovered a new phenomenon referred to as mitochondrial superoxide flashes (mSOF) in which stochastic, quantal bursts of O_2^- are produced on a quiescent background within a variety of cell types (Wang et al., 2008; Pouvreau, 2010; Wei et al., 2011; Fang et al., 2011). mSOF are temporally associated with observed mitochondrial depolarizations but the mechanistic details however, remain unknown. More recently, links have been made between mSOF

frequency and longevity of a variety of *C. elegans* models by which mSOF frequency was negatively correlated with lifespan (Shen et al., 2014).

While the existence of these superoxide flashes is now well established there is a paucity of information concerning their physiological relevance and the regulatory and mechanistic details that govern their occurrence. As such, the first chapter of this thesis was designed to explore the characterization and use of recently identified redox and ROS sensitive fluorescent biosensors to detect these events while the latter sections focus on the exploration of potential regulatory and mechanistic details that govern their occurrence.

5.1 Characterization of a hydrogen peroxide specific fluorescent biosensor

While these mSOF have been investigated at the level of superoxide production these determinations are not able to reveal the physiological relevance of this phenomenon since superoxide is short lived (Wang et al., 2008; Pouvreau, 2010; Fang et al., 2011; Ma et al., 2011; Wei et al., 2011; Krebs and Roden, 2005; Zhang et al., 2013). Given the importance of mitochondrial redox and ROS signaling, the appropriateness of redox and hydrogen peroxide specific fluorescent biosensors for use in monitoring the occurrence of mSOF events was investigated. Hypothetically, this phenomenon may provide a mechanism by which the development of various ROS induced pathologies occur or may be predicted. While the expression of roGFPs in cells along with proper localization was possible we were unable to generate stable cell lines in which to characterize these sensors for use in monitoring superoxide flashes. We consequently, directed our focus to the use of pHyPer-dmito a mitochondrial targeted, hydrogen peroxide specific YFP for further consideration (Belousov et al., 2006).

If these flashes are sustained at the peroxide level perhaps they contribute to the key signaling mechanisms that govern a variety of processes and the development of various pathologies for which a role for ROS has been established. Our first main goal was to determine if this sensor was 1) sensitive enough and 2) capable of dynamic measurements on a timescale appropriate to document ROS flash events. Briefly, we were able to develop a microplate reader assay by which we could characterize both the sensitivity and the kinetics of the pHyPer-dmito biosensor in a cell free system. This then allowed us to assess its applicability in monitoring mitochondrial ROS flashes.

Microscopic analysis of subcellular localization was conducted following expression of the pHyPer-dmito probe in HEK293 cells. Results showed localization to the mitochondria and moderate baseline fluorescence, which would allow for dynamic measurements of H_2O_2 levels. Additionally, the development of stable HEK293-pHyPer-dmito cells facilitated by antibiotic selection and FACS provided us with a model system in which to carry out characterization of this sensor.

Previously, this biosensor was characterized as a peroxide specific biosensor and its ability to be localized to various subcellular compartments, responsive to exogenous H_2O_2 and ability to monitor changes in H_2O_2 levels was confirmed (Belousov et al., 2006; Malinouski et al., 2011). We set out to corroborate some of these initial findings with the use of this newly developed microplate reader assay. We showed that pHyPer-dmito is a reversible probe capable of monitoring spatial and temporal changes in H_2O_2 flux in a cell free system in the low micromolar range. It is clear from these determinations that pHyPer-

dmito is sensitive enough to detect the small changes in H_2O_2 levels expected to occur following dismutation of $O_2^{\cdot-}$ bursts. Similarly, its V_{max} for oxidation suggests it is able to identify the increases in ROS during these events.

Additionally, we were able to confirm the reversibility of the sensor as previously shown by Malinouski *et al* (2011). However, it is important to note that the characterization carried out by this group indicated the ability of 4,4'-dithiodipyridine and dithiothreitol (DTT) to reduce this biosensor (Malinouski et al., 2011). DTT is a strong reductant (redox potential =-330mV, pH 7) that is commonly used to alter redox conditions in *in vitro* systems. In our studies, we found the kinetics of the reduction of the sensor remained unchanged by the addition of large amounts of DTT. As such it can be concluded that the reversibility of this biosensor is dependent on endogenous enzymatic and non-enzymatic redox systems that exist in the cell, such as the thioredoxin and glutathione systems. Unfortunately, the kinetics of pHyPer-dmito reduction proved to be much slower than that observed during its oxidation; specifically we observed reduction occurring over ~30-40mins (*i.e.*, following the oxidation of the sensor by peroxide). Consequently, we conclude that this sensor is unable to detect the decay of ROS which occurs over ~15s with an exponential decay constant of ~8s.

While this probe is sufficiently sensitive for mSOF measurements, the kinetics of its reversibility via its reduction are too slow to monitor the quick dynamics of these short ~15-25 s bursts. As such it was necessary to identify another probe that might allow us to study mitochondrial ROS flash events in the context of mitochondrial uncoupling. We then began

working with the previously established mt-cpYFP probe to investigate the role of UCP3 in this phenomenon (Wang et al., 2008; Schwarzlander et al., 2012; Wei-LaPierre et al., 2013).

5.2 Elucidating a role for UCP3 in modulating mSOF

While the existence and key components of mSOF have been established, it still remains controversial as to how these events are regulated. It was believed there was a role for mPTP in their modulation through regulating the mitochondrial depolarizations associated with superoxide flashes based on appropriately observed changed in mSOF frequency with use of mPTP activators and inhibitors (Wang et al., 2008). However, additional studies have been unable to replicate these results (Pouvreau, 2010).

Given that uncoupling proteins (2 and 3) are activated by ROS and are expressed in a variety of cell types displaying mSOF, it is conceivable that they play a role in regulating these events (Mailloux et al., 2011). If UCP3 plays a role in their modulation then it is predicted their characteristics are altered in muscle tissue lacking UCP3. As such, our second main goal was to elucidate a role for UCP3 in governing mSOF through regulating the apparent temporally linked mitochondrial depolarizations.

Determinations of mSOF frequency and other characteristics carried out in WT and UCP3KO muscle showed that significant differences exist in duration of flash activity, which is prolonged in the absence of UCP3 ($n=4$, $p=0.04$), and in flash area ($n=4$, $p<0.01$), which is reduced in the absence of UCP3. While an increase in duration is in accordance with the hypothesis that UCP3 can control mSOF, the difference in size is curious. We thus used electron microscopy to quantify the average mitochondria area in skeletal muscle of these

mice. We aimed to determine if the observed difference in size was due to inherent differences in levels of mitochondrial size. Results confirmed that mitochondria in UCP3KO FDB were in fact smaller than their WT counterparts, implicating the smaller area for observed mSOF known to occur in mitochondria. This result was noted to be age dependent with no difference in mitochondrial size seen in younger mice (data not shown). It has been previously shown that UCP3KO mice exhibit impaired ROS handling and additionally that increase mitochondrial oxidative stress causes enhanced fragmentation via differential modulation of mitochondrial fission-fusion proteins (Wu et al., 2011).

While a complete abolition of mSOF was not seen in UCP3KO muscle additional information is required to fully discern the mechanistic details of this pheonomenon. However, as with many regulatory mechanisms redundancy exists and perhaps UCP3 is one of a few or many mSOF modulators. Since there are as yet no known specific inhibitors or activators for UCP3 it is difficult to further discern a role for UCP3 in governing these events without more information about the mechanism.

5.3 Mechanistic evaluations of the temporally linked quantal bursts in superoxide production and mitochondrial depolarizations

Given the lack of data that exists with respect to describing this pheonomenon, we set out to further investigate the link between the quantal bursts in superoxide and the apparent temporally linked mitochondrial depolarizations. The initial report on mSOF noted that while mitochondrial depolarizations are known to occur naturally within cells, all quantal bursts in superoxide production identified as mSOF are accompanied by a temporally-linked

mitochondrial depolarization (Wang et al., 2008). As such we set out to further investigate the relationship between mSOF and the observed mitochondrial depolarizations.

Currently, two mechanisms have been proposed for the temporal linkage of mSOF and membrane depolarization, simply put, depolarization may either initiate or assist in terminating the burst in superoxide production. If UCP3 were in the inactive state, it could contribute to mechanisms initiating the flash; mechanistically this would involve a metabolically induced gradual hyperpolarization of the MIM, thereby increasing constitutive ROS production, which then in turn would activate UCP3 causing MIM depolarization. The latter would be observed as a decrease in TMRE signal, if TMRE were used in the non-quench mode. As a result of the depolarization, the ETC would be stimulated to restore membrane potential through increased ETC function. Increased ETC activity could result in increased electron (e^-) slippage causing mSOF. Alternatively, if UCP3 were acting in a mechanism to terminate mSOF, increases in ETC function result in slight hyperpolarization of the MIM. Hyperpolarization of the MIM causes increased electron slippage resulting in a measured burst of superoxide production. Subsequently activation of UCP3-mediated leak mechanisms would thus occur as a result of increased superoxide production and thereby induce depolarization of the MIM.

Firstly, we were able to unveil a novel correlation between the temporally linked quantal burst in superoxide and the observed depolarizations. Individual flash analyses showed that the absolute amplitude of these events was positively correlated (r^2=0.6847, $p<0.0001$) suggesting a direct relationship between these two components defining mSOF. This relationship has not been previously reported; however our finding does not elucidate

which of the proposed mechanisms of mSOF is correct thus additional determinations were required.

Studies to date have utilized confocal microscopy in order to measure mSOF and as of yet, published time series results do not have the temporal resolution required to discern the mechanism of mSOF. Given this, we decided to employ spinning disk confocal technology in order to increase the temporal resolution of imaging these bursts in superoxide production (using mt-cpYFP) and mitochondrial depolarizations (using TMRE) in order to discern the order of events that define mSOF. These determinations however lacked sufficient speed for discernment of events

5.4 Investigation of the contribution fiber type composition on mSOF characteristics

It is well established that mSOF are metabolically linked, specifically originating from the metabolically dependent production of superoxide by the ETC (Wang et al., 2008; Pouvreau, 2010; Zhang et al., 2013). To date determinations of flash activity have been limited to those conducted in isolated myofibers from FDB, primary rat cardiomyocytes, neuronal and neuroendocrine cells (Pouvreau, 2010; Wei et al., 2011; Fang et al., 2011). These determinations however, have not been compared since there is no golden standard for flash detection analyses. We utilize the MATLAB based command line prompt program "Flash Collector" (University of Rochester, NY) in order to carry out objective measurements of flash activity (Wei et al., 2011). Values obtained with these newly established methods were comparable to those previously determined.

Our aim in this final set of experiments was to compare mSOF frequency and characteristics among muscles having different metabolic characteristics. Skeletal muscle fiber type is described by the myosin heavy chain (MHC) expressed in the cell. This classification system is based on the MHC isoform expressed in the fiber. Fiber type composition of an entire muscle however, often exists on a spectrum with a tendency to be more focused on certain metabolic and functional capabilities.

MHCI expressing fibers are described as slow oxidative fibers. These fibers are slow twitch, have high resistance to fatigue, high mitochondrial content and rely predominantly on oxidative metabolism for the production of ATP(Pette and Staron, 2000). MHCII fibers can be further sub-classified by their two main isoforms MHCIIa and MHC IIb. MHC IIa muscle fibers are fast oxidative/glycolytic in nature. These are fast twitch fibers, which exhibit high resistance to fatigue, high mitochondrial content and rely generally on oxidative metabolism(Pette and Staron, 2000). MHC IIb fibers on the other hand are fast glycolytic in nature. These are fast twitch fibers, which demonstrate a low resistance to fatigue, low mitochondrial content and rely predominantly on glycolytic metabolism for ATP production(Pette and Staron, 2000).

Due to the known differences in metabolism, we investigated flash characteristics in muscle types displaying either a more oxidative or more glycolytic phenotype and compared the findings to the known values from FDB determinations. Soleus muscle was used as the oxidative muscle since roughly two thirds of its fibers rely mostly on oxidative metabolism (MHC I and MHC IIa) (Augusto et al., 2004). Conversely, EDL represents a more glycolytic phenotype with two thirds of its fibers relying mostly on glycolytic metabolism (Augusto et

al., 2004). The ability to carry out determinations in a variety of skeletal muscle types enables increased relevance of the results to studies, which may be conducted in primary cells isolated from other muscle types.

We are able to measure mSOF in fibers isolated from muscles characterized by large differences in fiber type composition. While the fiber type composition of soleus and EDL are majorly oxidative and glycolytic respectively their average mSOF frequencies and characteristics do not differ with any statistical significance. While muscles *in vivo* may be composed of fiber types, which confer either a more oxidative or more glycolytic metabolic phenotype, in culture, primary muscle cells revert to a mixed fiber type composition. As such the metabolic functionality of cultured myoblasts or myotubes may not be representative of what is observed *in vivo* (Pette and Staron, 2000).

These findings in light of fiber type differences perhaps indicate that these mSOF result from a low basal level of superoxide production in the isolated tissue. As such the potential importance of these events in governing ROS induced pathologies, which are not fiber type specific, remains high; however further investigations into the relationship between mSOF and these pathologies are required.

6.0 CONCLUSION:

In summation, this thesis provides new information about the kinetics of pHyPer-dmito and provides insight into the mechanism of skeletal muscle mSOF. Specifically, we show that while the sensitivity of pHyPer-dmito is sufficient to monitor subsequent dismutation of superoxide to H_2O_2 produced during mSOF the kinetics are insufficient. The development of a new hydrogen peroxide specific protein biosensor would indeed be helpful in elucidating whether mSOF are translated into sustained hydrogen peroxide flashes for a role in cell signaling processes. Using mt-cpYFP, we have identified a possible role for UCP3 in modulating characteristics of mSOF. While some mSOF characteristics were unchanged in the absence of UCP3 expression, analyses showed a prolonged duration of flashes in the UCP3KO muscle compared to WT muscle. Additionally, the average area of the flashes in UCP3KO mice was 30% smaller than that observed in WT mice; however, this finding was explained by intrinsic differences in mitochondrial size observed. In addition to these exciting findings we have unearthed a novel relationship between flash amplitude and mitochondrial depolarization supporting a role for mSOF regulation by these temporally linked mitochondrial depolarizations. Preliminary, investigations of mSOF characteristics among muscles of various fiber type compositions showed no difference in the frequency or characteristics of these metabolically linked events.

7.0 FUTURE WORK:

Given the described results, further research is needed to fully discern the mechanistic details of mSOF events. The current findings demonstrate a role for UCP3 in modulating flashes and a direct correlation between the amplitude of mSOF and temporally linked MIM depolarization. Future work should look into the potential of UCP3 specific inhibition or UCP3 mutagenesis in mt-cpYFP mice to further investigate this role as well as the use of spinning disk confocal technology for increased temporal resolution to discern mechanistic details of mSOF. Additionally, using primary myoblasts isolated from mt-cpYFP transgenic mice determinations in the presence of various substrates may elucidate a certain ROS production site within the ETC as the source of mSOF superoxide production.

In addition to these mechanistic determinations the physiological importance of mSOF, is yet to be defined. Findings by Shen *et al*. 2014 show a correlation between peaks in mSOF frequency and the lifespan of *C. elegans*. As such, a link between mSOF and the development of ROS induced pathologies should be investigated. Associations between heightened ROS production and the development of insulin resistance in muscle have been noted, however mechanistic details are lacking. Through use of mt-cpYFP in a high fat diet induced obesity mouse model as well as the use of primary myoblasts isolated from patients with a family history of T2DM the mechanistic details of how these pathologies develop and the role of mSOF in their development should be investigated.

8.0 REFERENCES:

Adam-Vizi, V., and L. Tretter. (2013). The role of mitochondrial dehydrogenases in the generation of oxidative stress. Neurochemistry International. 62, 757-763.

Affourtit, C., P.G. Crichton, N. Parker, et al. (2007). Novel uncoupling proteins. Novartis Foundation Symposium. 287, 70-80; discussion 80-91.

Aguer, C., O. Fiehn, E.L. Seifert, et al. (2013). Muscle uncoupling protein 3 overexpression mimics endurance training and reduces circulating biomarkers of incomplete beta-oxidation. FASEB Journal : Official Publication of the Federation of American Societies for Experimental Biology. 27, 4213-4225.

Anderson, E.J., M.E. Lustig, K.E. Boyle, et al. (2009). Mitochondrial H2O2 emission and cellular redox state link excess fat intake to insulin resistance in both rodents and humans. The Journal of Clinical Investigation. 119, 573-581.

Argyropoulos, G., A.M. Brown, S.M. Willi, et al. (1998). Effects of mutations in the human uncoupling protein 3 gene on the respiratory quotient and fat oxidation in severe obesity and type 2 diabetes. The Journal of Clinical Investigation. 102, 1345-1351.

Argyropoulos, G., and M.E. Harper. (2002). Uncoupling proteins and thermoregulation. Journal of Applied Physiology (Bethesda, Md.: 1985). 92, 2187-2198.

Augusto, V., C.R. Padvoani, and G.E.R. Campos. (2004). Skeletal muscle fiber types in C57Bl6J mice. Brazil Journal of Morphological Science. 21, 89-94.

Bayir, H., and V.E. Kagan. (2008). Bench-to-bedside review: Mitochondrial injury, oxidative stress and apoptosis--there is nothing more practical than a good theory. Critical Care (London, England). 12, 206.

Belousov, V.V., A.F. Fradkov, K.A. Lukyanov, et al. (2006). Genetically encoded fluorescent indicator for intracellular hydrogen peroxide. Nature Methods. 3, 281-286.

Berardi, M.J., W.M. Shih, S.C. Harrison, et al. (2011). Mitochondrial uncoupling protein 2 structure determined by NMR molecular fragment searching. Nature. 476, 109-113.

Bezaire, V., L.L. Spriet, S. Campbell, et al. (2005). Constitutive UCP3 overexpression at physiological levels increases mouse skeletal muscle capacity for fatty acid transport and oxidation. FASEB Journal : Official Publication of the Federation of American Societies for Experimental Biology. 19, 977-979.

Boss, O., S. Samec, A. Paoloni-Giacobino, et al. (1997). Uncoupling protein-3: a new member of the mitochondrial carrier family with tissue-specific expression. FEBS Letters. 408, 39-42.

Brand, M.D., K.M. Brindle, J.A. Buckingham, et al. (1999). The significance and mechanism of mitochondrial proton conductance. International Journal of Obesity and Related Metabolic Disorders : Journal of the International Association for the Study of Obesity. 23 Suppl 6, S4-11.

Brand, M.D., and D.G. Nicholls. (2011). Assessing mitochondrial dysfunction in cells. The Biochemical Journal. 435, 297-312.

Brand, M.D., J.L. Pakay, A. Ocloo, et al. (2005). The basal proton conductance of mitochondria depends on adenine nucleotide translocase content. The Biochemical Journal. 392, 353-362.

Bray, G.A., and D.H. Ryan. (2012). Medical therapy for the patient with obesity. Circulation. 125, 1695-1703.

Chan, C.B., and M.E. Harper. (2006). Uncoupling proteins: role in insulin resistance and insulin insufficiency. Current Diabetes Reviews. 2, 271-283.

Chang, K.C., C.C. Hsu, S.H. Liu, et al. (2013). Cadmium induces apoptosis in pancreatic beta-cells through a mitochondria-dependent pathway: the role of oxidative stress-mediated c-Jun N-terminal kinase activation. PloS One. 8, e54374.

Chen, X., S. Wei, and F. Yang. (2012). Mitochondria in the pathogenesis of diabetes: a proteomic view. Protein & Cell. 3, 648-660.

Choi, H., S. Kim, P. Mukhopadhyay, et al. (2001). Structural basis of the redox switch in the OxyR transcription factor. Cell. 105, 103-113.

Costford, S.R., S.N. Chaudhry, S.A. Crawford, et al. (2008). Long-term high-fat feeding induces greater fat storage in mice lacking UCP3. American Journal of Physiology.Endocrinology and Metabolism. 295, E1018-24.

Costford, S.R., S.N. Chaudhry, M. Salkhordeh, et al. (2006). Effects of the presence, absence, and overexpression of uncoupling protein-3 on adiposity and fuel metabolism in congenic mice. American Journal of Physiology.Endocrinology and Metabolism. 290, E1304-12.

Dikalov, S.I., and D.G. Harrison. (2012). Methods for detection of mitochondrial and cellular ROS. Antioxidants & Redox Signaling.

Eaton, S. (2002). Control of mitochondrial beta-oxidation flux. Progress in Lipid Research. 41, 197-239.

Echtay, K.S., T.C. Esteves, J.L. Pakay, et al. (2003). A signalling role for 4-hydroxy-2-nonenal in regulation of mitochondrial uncoupling. The EMBO Journal. 22, 4103-4110.

Echtay, K.S., D. Roussel, J. St-Pierre, et al. (2002). Superoxide activates mitochondrial uncoupling proteins. Nature. 415, 96-99.

Estey, C., E.L. Seifert, C. Aguer, et al. (2012). Calorie restriction in mice overexpressing UCP3: evidence that prior mitochondrial uncoupling alters response. Experimental Gerontology. 47, 361-371.

Fang, H., M. Chen, Y. Ding, et al. (2011). Imaging superoxide flash and metabolism-coupled mitochondrial permeability transition in living animals. Cell Research. 21, 1295-1304.

Ferrick, D.A., A. Neilson, and C. Beeson. (2008). Advances in measuring cellular bioenergetics using extracellular flux. Drug Discovery Today. 13, 268-274.

Fleury, C., M. Neverova, S. Collins, et al. (1997). Uncoupling protein-2: a novel gene linked to obesity and hyperinsulinemia. Nature Genetics. 15, 269-272.

Forman, H.J., and J. Kennedy. (1975). Superoxide production and electron transport in mitochondrial oxidation of dihydroorotic acid. The Journal of Biological Chemistry. 250, 4322-4326.

Garcia, N., C. Zazueta, R. Carrillo, et al. (2000). Copper sensitizes the mitochondrial permeability transition to carboxytractyloside and oleate. Molecular and Cellular Biochemistry. 209, 119-123.

Gellerich, F.N., Z. Gizatullina, T. Gainutdinov, et al. (2013). The control of brain mitochondrial energization by cytosolic calcium: the mitochondrial gas pedal. IUBMB Life. 65, 180-190.

Giorgio, M., E. Migliaccio, F. Orsini, et al. (2005). Electron transfer between cytochrome c and p66Shc generates reactive oxygen species that trigger mitochondrial apoptosis. Cell. 122, 221-233.

Gong, D.W., S. Monemdjou, O. Gavrilova, et al. (2000). Lack of obesity and normal response to fasting and thyroid hormone in mice lacking uncoupling protein-3. The Journal of Biological Chemistry. 275, 16251-16257.

Gunner, M.R., J. Madeo, and Z. Zhu. (2008). Modification of quinone electrochemistry by the proteins in the biological electron transfer chains: examples from photosynthetic reaction centers. Journal of Bioenergetics and Biomembranes. 40, 509-519.

Gutscher, M., A.L. Pauleau, L. Marty, et al. (2008). Real-time imaging of the intracellular glutathione redox potential. Nature Methods. 5, 553-559.

Guzy, R.D., and P.T. Schumacker. (2006). Oxygen sensing by mitochondria at complex III: the paradox of increased reactive oxygen species during hypoxia. Experimental Physiology. 91, 807-819.

Harmancey, R., H.G. Vasquez, P.H. Guthrie, et al. (2013). Decreased long-chain fatty acid oxidation impairs postischemic recovery of the insulin-resistant rat heart. FASEB Journal : Official Publication of the Federation of American Societies for Experimental Biology. 27, 3966-3978.

Harper, J.A., K. Dickinson, and M.D. Brand. (2001). Mitochondrial uncoupling as a target for drug development for the treatment of obesity. Obesity Reviews : An Official Journal of the International Association for the Study of Obesity. 2, 255-265.

Harper, M.E., R. Dent, S. Monemdjou, et al. (2002). Decreased mitochondrial proton leak and reduced expression of uncoupling protein 3 in skeletal muscle of obese diet-resistant women. Diabetes. 51, 2459-2466.

Harper, M.E., K. Green, and M.D. Brand. (2008). The efficiency of cellular energy transduction and its implications for obesity. Annual Review of Nutrition. 28, 13-33.

Himms-Hagen, J. (1990). Brown adipose tissue thermogenesis: interdisciplinary studies. FASEB Journal : Official Publication of the Federation of American Societies for Experimental Biology. 4, 2890-2898.

Himms-Hagen, J. (1989). Role of thermogenesis in the regulation of energy balance in relation to obesity. Canadian Journal of Physiology and Pharmacology. 67, 394-401.

Hirst, J., M.S. King, and K.R. Pryde. (2008). The production of reactive oxygen species by complex I. Biochemical Society Transactions. 36, 976-980.

Hoeks, J., M.K. Hesselink, M. van Bilsen, et al. (2003). Differential response of UCP3 to medium versus long chain triacylglycerols; manifestation of a functional adaptation. FEBS Letters. 555, 631-637.

Houstis, N., E.D. Rosen, and E.S. Lander. (2006). Reactive oxygen species have a causal role in multiple forms of insulin resistance. Nature. 440, 944-948.

Huang, Z., W. Zhang, H. Fang, et al. (2011). Response to "A critical evaluation of cpYFP as a probe for superoxide". Free Radical Biology & Medicine. 51, 1937-1940.

Jastroch, M., A.S. Divakaruni, S. Mookerjee, et al. (2010). Mitochondrial proton and electron leaks. Essays in Biochemistry. 47, 53-67.

Koehler, C.M., K.N. Beverly, and E.P. Leverich. (2006). Redox pathways of the mitochondrion. Antioxidants & Redox Signaling. 8, 813-822.

Krebs, M., and M. Roden. (2005). Molecular mechanisms of lipid-induced insulin resistance in muscle, liver and vasculature. Diabetes, Obesity & Metabolism. 7, 621-632.

Krook, A., J. Digby, S. O'Rahilly, et al. (1998). Uncoupling protein 3 is reduced in skeletal muscle of NIDDM patients. Diabetes. 47, 1528-1531.

Lambert, A.J., and M.D. Brand. (2004a). Inhibitors of the quinone-binding site allow rapid superoxide production from mitochondrial NADH:ubiquinone oxidoreductase (complex I). The Journal of Biological Chemistry. 279, 39414-39420.

Lambert, A.J., and M.D. Brand. (2004b). Superoxide production by NADH:ubiquinone oxidoreductase (complex I) depends on the pH gradient across the mitochondrial inner membrane. The Biochemical Journal. 382, 511-517.

Lenaz, G. (2001). The mitochondrial production of reactive oxygen species: mechanisms and implications in human pathology. IUBMB Life. 52, 159-164.

Lengacher, S., P.J. Magistretti, and L. Pellerin. (2004). Quantitative rt-PCR analysis of uncoupling protein isoforms in mouse brain cortex: methodological optimization and comparison of expression with brown adipose tissue and skeletal muscle. Journal of Cerebral Blood Flow and Metabolism : Official Journal of the International Society of Cerebral Blood Flow and Metabolism. 24, 780-788.

Li, N., B. Li, T. Brun, et al. (2012). NADPH Oxidase NOX2 Defines a New Antagonistic Role for Reactive Oxygen Species and cAMP/PKA in the Regulation of Insulin Secretion. Diabetes.

Loschen, G., A. Azzi, and L. Flohe. (1973). Mitochondrial H2O2 formation: relationship with energy conservation. FEBS Letters. 33, 84-87.

Ma, Q., H. Fang, W. Shang, et al. (2011). Superoxide flashes: early mitochondrial signals for oxidative stress-induced apoptosis. The Journal of Biological Chemistry. 286, 27573-27581.

MacLellan, J.D., M.F. Gerrits, A. Gowing, et al. (2005). Physiological increases in uncoupling protein 3 augment fatty acid oxidation and decrease reactive oxygen species production without uncoupling respiration in muscle cells. Diabetes. 54, 2343-2350.

Madeira, V.M. (2012). Overview of mitochondrial bioenergetics. Methods in Molecular Biology (Clifton, N.J.). 810, 1-6.

Mailloux, R.J., C.N. Adjeitey, and M.E. Harper. (2010). Genipin-induced inhibition of uncoupling protein-2 sensitizes drug-resistant cancer cells to cytotoxic agents. PloS One. 5, e13289.

Mailloux, R.J., A. Fu, C. Robson-Doucette, et al. (2012). Glutathionylation state of uncoupling protein-2 and the control of glucose-stimulated insulin secretion. The Journal of Biological Chemistry. 287, 39673-39685.

Mailloux, R.J., and M.E. Harper. (2011). Uncoupling proteins and the control of mitochondrial reactive oxygen species production. Free Radical Biology & Medicine. 51, 1106-1115.

Mailloux, R.J., E.L. Seifert, F. Bouillaud, et al. (2011). Glutathionylation acts as a control switch for uncoupling proteins UCP2 and UCP3. The Journal of Biological Chemistry. 286, 21865-21875.

Malinouski, M., Y. Zhou, V.V. Belousov, et al. (2011). Hydrogen peroxide probes directed to different cellular compartments. PloS One. 6, e14564.

Mao, W., X.X. Yu, A. Zhong, et al. (1999). UCP4, a novel brain-specific mitochondrial protein that reduces membrane potential in mammalian cells. FEBS Letters. 443, 326-330.

Matthias, A., A. Jacobsson, B. Cannon, et al. (1999). The bioenergetics of brown fat mitochondria from UCP1-ablated mice. Ucp1 is not involved in fatty acid-induced de-energization ("uncoupling"). The Journal of Biological Chemistry. 274, 28150-28160.

Mesecke, N., N. Terziyska, C. Kozany, et al. (2005). A disulfide relay system in the intermembrane space of mitochondria that mediates protein import. Cell. 121, 1059-1069.

Meyer, A.J., and T.P. Dick. (2010a). Fluorescent protein-based redox probes. Antioxidants & Redox Signaling. 13, 621-650.

Mitchell, P. (2011). Chemiosmotic coupling in oxidative and photosynthetic phosphorylation. 1966. Biochimica Et Biophysica Acta. 1807, 1507-1538.

Mitchell, P. (1972). Chemiosmotic coupling in energy transduction: a logical development of biochemical knowledge. Journal of Bioenergetics. 3, 5-24.

Mitchell, P. (1966). Chemiosmotic coupling in oxidative and photosynthetic phosphorylation. Biological Reviews of the Cambridge Philosophical Society. 41, 445-502.

Mitchell, P. (1961). Coupling of phosphorylation to electron and hydrogen transfer by a chemi-osmotic type of mechanism. Nature. 191, 144-148.

Muller, F.L., Y. Liu, and H. Van Remmen. (2004). Complex III releases superoxide to both sides of the inner mitochondrial membrane. The Journal of Biological Chemistry. 279, 49064-49073.

Murphy, M.P. (2009). How mitochondria produce reactive oxygen species. The Biochemical Journal. 417, 1-13.

Pette, D., and R.S. Staron. (2000). Myosin isoforms, muscle fiber types, and transitions. Microscopy Research and Technique. 50, 500-509.

Pouvreau, S. (2010). Superoxide flashes in mouse skeletal muscle are produced by discrete arrays of active mitochondria operating coherently. PloS One. 5, e13035.

Pryde, K.R., and J. Hirst. (2011). Superoxide is produced by the reduced flavin in mitochondrial complex I: a single, unified mechanism that applies during both forward and reverse electron transfer. The Journal of Biological Chemistry. 286, 18056-18065.

Quinlan, C.L., A.L. Orr, I.V. Perevoshchikova, et al. (2012). Mitochondrial Complex II Can Generate Reactive Oxygen Species at High Rates in Both the Forward and Reverse Reactions. The Journal of Biological Chemistry. 287, 27255-27264.

Ralph, S.J., R. Moreno-Sanchez, J. Neuzil, et al. (2011). Inhibitors of succinate: quinone reductase/Complex II regulate production of mitochondrial reactive oxygen species and protect normal cells from ischemic damage but induce specific cancer cell death. Pharmaceutical Research. 28, 2695-2730.

Ricquier, D., and F. Bouillaud. (2000). The uncoupling protein homologues: UCP1, UCP2, UCP3, StUCP and AtUCP. The Biochemical Journal. 345 Pt 2, 161-179.

Ricquier, D., C. Lin, and M. Klingenberg. (1982). Isolation of the GDP binding protein from brown adipose tissue mitochondria of several animals and amino acid composition study in rat. Biochemical and Biophysical Research Communications. 106, 582-589.

Rinaldo, P., D. Matern, and M.J. Bennett. (2002). Fatty acid oxidation disorders. Annual Review of Physiology. 64, 477-502.

Rolfe, D.F., and M.D. Brand. (1996). Contribution of mitochondrial proton leak to skeletal muscle respiration and to standard metabolic rate. The American Journal of Physiology. 271, C1380-9.

Rolfe, D.F., J.M. Newman, J.A. Buckingham, et al. (1999). Contribution of mitochondrial proton leak to respiration rate in working skeletal muscle and liver and to SMR. The American Journal of Physiology. 276, C692-9.

Sanchis, D., C. Fleury, N. Chomiki, et al. (1998). BMCP1, a novel mitochondrial carrier with high expression in the central nervous system of humans and rodents, and respiration uncoupling activity in recombinant yeast. The Journal of Biological Chemistry. 273, 34611-34615.

Schagger, H., R. de Coo, M.F. Bauer, et al. (2004). Significance of respirasomes for the assembly/stability of human respiratory chain complex I. The Journal of Biological Chemistry. 279, 36349-36353.

Schrauwen, P., M.K. Hesselink, E.E. Blaak, et al. (2001). Uncoupling protein 3 content is decreased in skeletal muscle of patients with type 2 diabetes. Diabetes. 50, 2870-2873.

Schrauwen, P., M. Mensink, G. Schaart, et al. (2006). Reduced skeletal muscle uncoupling protein-3 content in prediabetic subjects and type 2 diabetic patients: restoration by rosiglitazone treatment. The Journal of Clinical Endocrinology and Metabolism. 91, 1520-1525.

Schwarzlander, M., M.P. Murphy, M.R. Duchen, et al. (2012). Mitochondrial 'flashes': a radical concept repHined. Trends in Cell Biology.

Scialo, F., V. Mallikarjun, R. Stefanatos, et al. (2013). Regulation of lifespan by the mitochondrial electron transport chain: reactive oxygen species-dependent and reactive oxygen species-independent mechanisms. Antioxidants & Redox Signaling. 19, 1953-1969.

Seifert, E.L., C. Estey, J.Y. Xuan, et al. (2010). Electron transport chain-dependent and -independent mechanisms of mitochondrial H2O2 emission during long-chain fatty acid oxidation. The Journal of Biological Chemistry. 285, 5748-5758.

Shen, E.Z., C.Q. Song, Y. Lin, et al. (2014). Mitoflash frequency in early adulthood predicts lifespan in Caenorhabditis elegans. Nature. 508, 128-132.

Sluse, F.E. (2012). Uncoupling proteins: molecular, functional, regulatory, physiological and pathological aspects. Advances in Experimental Medicine and Biology. 942, 137-156.

Song, J.X., M.Y. Choi, K.C. Wong, et al. (2012). Baicalein antagonizes rotenone-induced apoptosis in dopaminergic SH-SY5Y cells related to Parkinsonism. Chinese Medicine. 7, 1-8546-7-1.

Starkov, A.A., G. Fiskum, C. Chinopoulos, et al. (2004). Mitochondrial alpha-ketoglutarate dehydrogenase complex generates reactive oxygen species. The Journal of Neuroscience : The Official Journal of the Society for Neuroscience. 24, 7779-7788.

St-Pierre, J., J.A. Buckingham, S.J. Roebuck, et al. (2002). Topology of superoxide production from different sites in the mitochondrial electron transport chain. The Journal of Biological Chemistry. 277, 44784-44790.

Takeshige, K., and S. Minakami. (1979). NADH- and NADPH-dependent formation of superoxide anions by bovine heart submitochondrial particles and NADH-ubiquinone reductase preparation. The Biochemical Journal. 180, 129-135.

Tormos, K.V., E. Anso, R.B. Hamanaka, et al. (2011). Mitochondrial complex III ROS regulate adipocyte differentiation. Cell Metabolism. 14, 537-544.

Tretter, L., and V. Adam-Vizi. (2004). Generation of reactive oxygen species in the reaction catalyzed by alpha-ketoglutarate dehydrogenase. The Journal of Neuroscience : The Official Journal of the Society for Neuroscience. 24, 7771-7778.

Tretter, L., K. Takacs, V. Hegedus, et al. (2007). Characteristics of alpha-glycerophosphate-evoked H2O2 generation in brain mitochondria. Journal of Neurochemistry. 100, 650-663.

Vidal-Puig, A., G. Solanes, D. Grujic, et al. (1997). UCP3: an uncoupling protein homologue expressed preferentially and abundantly in skeletal muscle and brown adipose tissue. Biochemical and Biophysical Research Communications. 235, 79-82.

Vidal-Puig, A.J., D. Grujic, C.Y. Zhang, et al. (2000). Energy metabolism in uncoupling protein 3 gene knockout mice. The Journal of Biological Chemistry. 275, 16258-16266.

Wang, W., H. Fang, L. Groom, et al. (2008). Superoxide flashes in single mitochondria. Cell. 134, 279-290.

Wei, L., and R.T. Dirksen. (2012). Perspectives on: SGP symposium on mitochondrial physiology and medicine: mitochondrial superoxide flashes: from discovery to new controversies. The Journal of General Physiology. 139, 425-434.

Wei, L., G. Salahura, S. Boncompagni, et al. (2011). Mitochondrial superoxide flashes: metabolic biomarkers of skeletal muscle activity and disease. FASEB Journal : Official Publication of the Federation of American Societies for Experimental Biology. 25, 3068-3078.

Wei-LaPierre, L., G. Gong, B.J. Gerstner, et al. (2013). Respective contribution of mitochondrial superoxide and pH to mitochondria-targeted circularly permuted yellow fluorescent protein (mt-cpYFP) flash activity. The Journal of Biological Chemistry. 288, 10567-10577.

Wu, S., F. Zhou, Z. Zhang, et al. (2011). Mitochondrial oxidative stress causes mitochondrial fragmentation via differential modulation of mitochondrial fission-fusion proteins. The FEBS Journal. 278, 941-954.

Yu, X.X., J.L. Barger, B.B. Boyer, et al. (2000). Impact of endotoxin on UCP homolog mRNA abundance, thermoregulation, and mitochondrial proton leak kinetics. American Journal of Physiology.Endocrinology and Metabolism. 279, E433-46.

Zhang, X., Z. Huang, T. Hou, et al. (2013). Superoxide constitutes a major signal of mitochondrial superoxide flash. Life Sciences. 93, 178-186.

Zheng, M., F. Aslund, and G. Storz. (1998). Activation of the OxyR transcription factor by reversible disulfide bond formation. Science (New York, N.Y.). 279, 1718-1721.

Zundorf, G., S. Kahlert, V.I. Bunik, et al. (2009). alpha-Ketoglutarate dehydrogenase contributes to production of reactive oxygen species in glutamate-stimulated hippocampal neurons in situ. Neuroscience. 158, 610-616.

9.0 CURRICULUM VITAE:

Skye McBride

SUMMARY OF QUALIFICATIONS

- MSc Biochemistry, University of Ottawa (Supervisor: Dr. M-E Harper)- Expected graduation August 2014
- Two years additional work experience in Biochemistry and Molecular Genetics
- Author on four primary research one review article
- Supervisorial experience for multiple undergraduate and summer students
- Volunteer and work experience related to science teaching, training and communication
- Completion of Community Outreach and Media Relations in the Science Communications course
- Fluent in English, intermediate working proficiency in French

AWARDS, HONOURS AND ACCOLADES

- University of Ottawa Biochemistry, Microbiology and Immunology seminar- 1st place (MSc Biochemistry) -2014
- Excellence Scholarship University of Ottawa- 2012/13, 2013/14
- Ontario Graduate Scholarship (OGS)-2012/13 (Declined), 2013/14
- Research Travel Grant- 2013
- NSERC Canada Graduate Scholarship (CGS-M) 2012/13
- Natural Sciences and Engineering Research Council of Canada (NSERC) Undergraduate Summer Research Award (USRA) Carleton University- 2010, 2011. University of Ottawa 2012
- Senate Medal Recipient Carleton University- 2012
- Geoff Wightman Award in Chemistry-2011/12
- Dean's Summer Research Internship (DSRI) Carleton University 2009
- Richard Lewar Prestige Scholarship Carleton University, 2008/09-2011/12
- Faculty of Science Scholarship- 2008/09

WORK EXPERIENCE

Teaching Assistant Ottawa, ON

University of Ottawa (General Intermediary Metabolism)	Jan 2014- Apr 2014
Carleton University (Introductory Genetics)	Sept 2011-Apr 2012
Carleton University (Organic Chemistry I/II)	July 2011-Aug 2011

- Respond to student questions regarding course material
- Proctor and mark all midterms and final exam
- Held tutorial and review sessions for midterms and final exam

Research Assistant Ottawa, ON

University of Ottawa, Faculty of Medicine (Dr. M-E Harper)	May 2012- Aug 2012
Carleton University, Institute of Biochemistry (Dr. W Willmore)	May 2011 - Apr 2012
Carleton University, Institute of Biochemistry (Dr. W Willmore)	May 2010- Aug 2010

Carleton University, Department of Chemistry (Dr. Z Wang) May 2009- Aug 2009

- Designed, executed, analysed and interpreted all experiments related to an independent research project
- Communicated results through written reports, posters and seminar talks

Office Administration and Customer Relations Lansdowne, ON
Misty Isles Lodge www.mistyisles.ca (O/O Gayle Grant) May 2003-Aug 2008

- Performed office administration duties
- Communicated clearly with customers
- Instructed guests in the operation of kayaks and motor boats

EDUCATION AND TRAINING

Master of Science, Biochemistry (Submitted) Sept 2012-Aug 2014
University of Ottawa, Ottawa, ON

- 10.0 CGPA (10.0 point scale)

Thesis: Elucidating a Role for UCP3 in the Control of Mitochondrial Superoxide Flashes

Bachelor of Science Honours, Biochemistry and Biotechnology Sept 2008– April 2012
Carleton University, Ottawa, ON

- Overall 11.625 CGPA (12.0 point scale)
- Last two years 11.90 CGPA (12.0 point scale)
- Thesis: p23 and processing of NFE2L1 (Nrf1) by the proteasome

VOLUNTEER EXPERIENCE

Medical/Dental Brigader Ottawa, ON
University of Ottawa Global Brigades (UOGB) club Sept 2013-May 2014

- Organized and participated in personal and club fundraisers
- Communicated with patients, doctors, dentists and support staff
- Maintained continued workflow through brigade stations

Expert on Demand Virtual
Partners in Research, Virtual Researchers On Call (VROC) Jan 2013-Present

- Liaise with elementary and high school educators in Canada
- Communicate via teleconference for enhanced in-classroom learning
- Participate in planning/hosting VROC STEM Camp at Western University 2013 and across 10 sites 2014

Science Outreach Volunteer Ottawa, ON
Let's Talk Science Sept 2012-Present

- Liaise with elementary and high school educators in Ottawa.
- Promote science to students through teaching and hands-on demonstrations

Member at Large Ottawa, ON Sept 2012-Present
Biochemistry, Microbiology and Immunology Graduate Student Association (BMIGSA)

- Liaise with students in the departments

- Communicate with BMIGSA representatives to voice student opinions
- Participate in planning/hosting events put on by the BMIGSA

High School Outreach Volunteer Ottawa, ON
Carleton University, Department of Biology November 2010
- Organized poster displays
- Explained opportunities for young researchers during university
- Answered questions about the biology and biochemistry programs at Carleton University

Program Initiative Coordinator Gananoque, ON
Gananoque Youth Centre (GYC) Sept 2006-Aug 2009
- Organized science, homework, cooking and camping programs for children

Quality Care Team Member Gananoque, ON
Gananoque Secondary School and Community volunteer Sept 2006-June 2007
- Managed meal time for quality care team for the disabled and elderly

ARTICLES IN REFEREED JOURNALS

Mailloux, R.J., Xuan, JY., **McBride, S**., Maharsy, W., Thorn, S., Holterman, CE., Kennedy, CRJ., Rippstein, P., deKemp, R., da Silva, J., Nemer, M., Lou, M. and Harper, M-E. Glutaredoxin-2 is Required to Control Oxidative Phosphorylation in Cardiac Muscle by Mediating Deglutathionylation Reactions. J. Biol. Chem. 2014. 21:14812-14828.

Mailloux, RJ., **McBride, SL** and Harper., M-E. Unearthing the secrets of mitochondrial ROS and glutathione in bioenergetics. TiBS. 2013. 38:592-602

Chepelev, N.L., Zhang, H., Liu, H., **McBride, S.**, Seal, A.J., Morgan, T.E., Finch, C.E., Willmore, W.G., Davies, K.J.A and Forman, H.J. Competition of nuclear factor-erythroid 2 factors related transcription factor isoforms, Nrf1 and Nrf2, in antioxidant enzyme induction. Redox. Biol., 2013. 1:183-189.

Chepelev, N.L., Bennitz, J.D., Huang, T., **McBride, S**., and Willmore, W.G. The Nrf1 CNC-bZIP protein is regulated by the proteasome and activated by hypoxia. PLoS ONE. 2011. 6(12): e29167.

Hao, W., McBride, W., **McBride, S**., Gao, J.P., and Wang, Z.Y. Colorimetric and near-infared fluorecence turn-on molecular probe for direct and highly selective detection of cysteine in human plasma. J. Mater. Chem., 2010. 21, 1040-1048.

CONFERENCES

McBride, S., Wei, L., Dirksen, R.T. and Harper, ME. Identification of a Role for Uncoupling Protein 3 in Modulating Mitochondrial Superoxide Flashes. Canadian Oxidative Stress Consortium 2014, 8th Annual Meeting.

REFERENCES

Dr. Mary-Ellen Harper, Full Professor, University of Ottawa – MSc Supervisor

Dr. William Willmore, Associate Professor, Carleton University-BSc Honours Supervisor